⌘ *Author's Choice*

THE JOURNAL OF BIOLOGICAL CHEMISTRY VOL. 287, NO. 52, pp. 43246–43261, December 21, 2012

Structural and Functional Characterization of the Kindlin-1 Pleckstrin Homology Domain*

Received for publication, September 25, 2012, and in revised form, October 21, 2012 Published, JBC Papers in Press, November 6, 2012, DOI 10.1074/jbc.M112.422089

Luke A. Yates[‡1], Craig N. Lumb[§1], Nina N. Brahme[¶‖], Ruta Zalyte[‡], Louise E. Bird[‡], Luigi De Colibus[‡], Raymond J. Owens[‡**], David A. Calderwood[¶‖], Mark S. P. Sansom[§], and Robert J. C. Gilbert[‡2]**

*From the [‡]Division of Structural Biology, Wellcome Trust Centre for Human Genetics, University of Oxford, Roosevelt Drive, Oxford OX3 7BN, United Kingdom, the [§]Department of Biochemistry, University of Oxford, South Parks Road, Oxford OX1 3QU, United Kingdom, the [¶]Department of Cell Biology and the [‖]Department of Pharmacology Yale University School of Medicine, New Haven, Connecticut 06520-8066, and the **Oxford Protein Production Facility United Kingdom, Research Complex at Harwell, Rutherford Appleton Laboratory, Harwell Oxford, Didcot OX11 0FA, United Kingdom*

Background: Kindlins are essential co-activators with talin of integrins.
Results: Kindlin-1 PH domain is necessary for integrin activation and has low affinity for PtdInsP species partly determined by a salt bridge across its binding pocket.
Conclusion: The PH domain is necessary to kindlins, localizing them to integrins, and displays subtle structural variations having major functional effects.
Significance: Targeting of kindlins partly depends on their PH domains.

Inside-out activation of integrins is mediated via the binding of talin and kindlin to integrin β-subunit cytoplasmic tails. The kindlin FERM domain is interrupted by a pleckstrin homology (PH) domain within its F2 subdomain. Here, we present data confirming the importance of the kindlin-1 PH domain for integrin activation and its x-ray crystal structure at a resolution of 2.1 Å revealing a C-terminal second α-helix integral to the domain but found only in the kindlin protein family. An isoform-specific salt bridge occludes the canonical phosphoinositide binding site, but molecular dynamics simulations display transient switching to an alternative open conformer. Molecular docking reveals that the opening of the pocket would enable potential ligands to bind within it. Although lipid overlay assays suggested the PH domain binds inositol monophosphates, surface plasmon resonance demonstrated weak affinities for inositol 3,4,5-triphosphate (Ins(3,4,5)P_3; K_D ~100 μM) and no monophosphate binding. Removing the salt bridge by site-directed mutagenesis increases the PH domain affinity for Ins(3,4,5)P_3 as measured by surface plasmon resonance and enables it to bind PtdIns(3,5)P_2 on a dot-blot. Structural comparison with other PH domains suggests that the phosphate binding pocket in the kindlin-1 PH domain is more occluded than in kindlins-2 and -3 due to its salt bridge. In addition, the apparent affinity for Ins(3,4,5)P_3 is affected by the presence of PO_4 ions in the buffer. We suggest the physiological ligand of the kindlin-1 PH domain is most likely not an inositol phosphate but another phosphorylated species.

The kindlin family of proteins has recently emerged as a crucial component of focal adhesion assembly, and they are, therefore, essential for complex life. Kindlins are considered co-activators of integrins alongside talin (1). Integrin-mediated cell adhesion connects the cell to the extracellular matrix in higher eukaryotes. It is a critical and common process in a plethora of physiological phenomena, which include tissue integrity, embryogenesis, bone metabolism, hemostasis, and immunity. The cytoplasmic tails of the integrin β-subunits that regulate integrin affinity for extracellular ligands can be divided into three regions, a membrane proximal region and two conserved N*XX*Y motifs (2). The N-terminal F3 subdomain of talin is known to bind to the more membrane proximal NP*X*Y (NPKY[747] in β3 integrin) motif resulting in enhanced activation (2–4). At the molecular level, the interaction of the talin F3 subdomain with this NP*X*Y motif results in the disruption of an intermolecular clasp that maintains integrins in a low affinity state (4). However, the more membrane distal N*XX*Y (NITY[759] in β3) motif and an intervening T/S (TST; S is Ser[752]) cluster are also critical for kindlin binding and integrin activation (3, 5, 6).

The mammalian kindlin family consists of 3 isoforms (kindlin-1, kindlin-2, and kindlin-3) with each exhibiting tissue-specific expression patterns. Kindlin-1 is expressed primarily in the epidermis but also to a lesser extent the colon, stomach, and kidneys. Kindlin-2 is ubiquitously expressed but concentrated in striated and smooth muscle, whereas kindlin-3 is expressed nearly exclusively in the hematopoietic tissues (7). Besides β integrins (6, 12–14), other kindlin binding partners include integrin-linked kinase (6, 8, 9) and migfilin (9–11). Additionally, kindlin-1 was shown to associate with both α-actinin and focal adhesion kinase (15), and kindlin-3 was shown to form a ternary complex with the kinase RACK1 and integrin β tails mediated by its PH[3] domain (16).

* This work was supported, in whole or in part, by National Institutes of Health Grants R01GM088240, R01 GM068600, and T32 GM007223 (to D. A. C. and N. N. B.). This work was also supported by the Biotechnology and Biological Sciences Research Council (United Kingdom) and the Wellcome Trust (to M. S. P. S.).
⌘ *Author's Choice*—Final version full access.
The atomic coordinates and structure factors (code 4bbk) have been deposited in the Protein Data Bank (http://wwpdb.org/).
[1] Supported by the Medical Research Council (UK) for financial support.
[2] A Royal Society University Research Fellow. To whom correspondence may be addressed. E-mail: gilbert@strubi.ox.ac.uk.

[3] The abbreviations used are: PH, pleckstrin homology; Ins(3,4,5)P_3, inositol 3,4,5-triphosphate; PtdIns(3,4,5)P_3, phosphatidylinositol 3,4,5-triphosphate; MFI, mean fluorescence intensity; r.m.s.d., root mean square deviation; SPR, surface plasmon resonance.

Loss-of-function mutations within the *FERMT1* (kindlin-1) gene in humans result in the rare recessive genodermatosis Kindler syndrome, characterized by transient skin blistering, skin atrophy, variegated hyper-pigmentation, and in some rare cases squamous cell carcinoma (17). Additionally, because of the expression of a kindlin-1 splice-variant in gastrointestinal tissues, Kindler syndrome-associated ulcerative colitis can also present in patients with Kindler syndrome (18). Loss of kindlin-2 (*FERMT2*) in murine models results in embryonic lethality; however, knockdown of kindlin-2 in zebrafish has revealed an important role for it in cardiac myocyte differentiation and morphogenesis (19). Studies show kindlin-3 knock-out mice ($KIND3^{-/-}$) suffer from severe bleeding due to inactive platelet integrins, which also results in fatal anemia because of additional erythrocytopenia (20). Loss of kindlin-3 (*FERMT3*) in humans results in leukocyte adhesion deficiency III (21). Individuals with leukocyte adhesion deficiency III suffer from Glanzmann's thrombasthenia-like bleeding disorders and recurrent infections, both of which are life threatening (22). More recently, biochemical and cell biological data have revealed a role for kindlin-3 in osteoclast podocyte formation, which is essential for bone resorption (23).

Recent studies have revealed that the pleckstrin homology (PH) domain of kindlin-2 binds multiple phosphoinositides, particularly phosphatidylinositol 3,4,5-triphosphate (PtdIns(3,4,5)P_3; $K_D \sim 2\ \mu$M), with a PH domain deletion or K390A mutant diminishing phosphoinositide binding (24). Furthermore, kindlin-2 was shown to localize to PtdIns(3,4,5)P_3-enriched membranes, and phosphoinositide binding-deficient kindlin-2 mutants were shown to impair podocyte integrin activation (25). Although this evidence suggests a molecular role for the kindlin-2 PH domain, differences in sequence to other isoforms suggest that other PH domains in the kindlin family may function distinctly. We, therefore, investigated the structure of the kindlin-1 PH domain to provide a molecular description of the domain and, with additional structural analysis, some clues as to its function in kindlin-1 biology.

EXPERIMENTAL PROCEDURES

Cloning and Expression—A DNA fragment corresponding to the PH domain of kindlin-1 (residues 364–509) was amplified by PCR from *Mus musculus FERMT1* cDNA, and DNA fragments for kindlin-2 (residues 367–512) and kindlin-3 (residues 344–495) PH domains were also amplified from mouse *FERMT2* and *FERMT3* cDNA, respectively (cDNA was a kind gift from R. Faessler, MPI, Martinsreid, Germany). The PCR products were subsequently cloned into the pOPINF vector (26), which encodes a cleavable (3C protease) expression and purification N-terminal hexahistidine tag using InFusion cloning (Clontech). Recombinant plasmid was amplified in *Escherichia coli* and purified using standard protocols. Successful cloning was assessed by diagnostic PCR and DNA sequencing (Geneservices, Oxford, UK). Human kindlin-1 ΔPH was generated by PCR and cloned into the pEGFP-C1 vector (Clontech). Mouse talin head (amino acid residues 1–433) was generated as previously described (5) and cloned into pDsRed-Monomer-C1 vector (Clontech).

Site-directed Mutagenesis—A single point mutation (E416A) was introduced using PCR-based mutagenesis with the primer 5′-AAACCTTAGAGGCTGCGCAATTGTGCCAGATGTGA-3′ and the complementary primer 5′-TCACATCTGGCACAATTGCGCAGCCTCTAAGGTTT-3′ using Phusion-Hot Start DNA polymerase (Finzymes). Subsequently, template DNA was digested with DpnI for 1 h at 37 °C. The PCR product was checked using 1% (w/v) agarose gel electrophoresis and used for transformation of *E. coli* for amplification using standard methods. DNA sequencing (Geneservices, Oxford, UK) was performed to verify the introduction of the mutant.

Integrin Activation Assay—Integrin activation assays were conducted and quantified as previously described (27). Briefly, CHO cells stably expressing αIIbβ3 integrins were transiently co-transfected with GFP- and DsRed-tagged constructs using PEI (Polysciences Inc.). Twenty-four hours later cells were suspended and stained with PAC1 (BD Biosciences) and Alexa 647 fluorophore-conjugated anti-mouse IgM secondary (Invitrogen) in the presence ("inhibited") and absence ("native") of 10 mM EDTA. Total surface integrin levels were measured by staining with D57 (28) and Alexa 647 fluorophore-conjugated anti-mouse IgG secondary (Invitrogen). Mean fluorescence intensities (MFI) of PAC1 and D57 binding were calculated using FlowJo FACS analysis software. The integrin activation index (AI) of GFP- and DsRed-positive cells in each experimental condition was quantified as AI = (native$_{MFI}$ − inhibited$_{MFI}$)/D57$_{MFI}$. Statistical significance was calculated using Student's *t* test.

Protein Expression and Purification—Recombinant kindlin-1 PH domain was, unusually, constitutively expressed; therefore *E. coli* Rosetta (pLysS/RARE) carrying recombinant plasmids were cultured in LB supplemented with ampicillin (50 μg/ml) and chloramphenicol (34 μg/ml) at 37 °C overnight with shaking (200 rpm). Cultures were diluted 1:1000 into Terrific broth supplemented with ampicillin and chloramphenicol and incubated at 37 °C with shaking at 200 rpm until saturation. Cells were harvested by centrifugation at 5000 × *g* for 20 min at 4 °C. The supernatant was decanted, and the pellet was resuspended in 50 mM Tris-HCl, pH 7.5, 20 mM imidazole, 500 mM NaCl, 0.2% (v/v) Tween at a ratio of 30 ml of buffer to 10 g of cell pellet. Resuspended cell pellets were stored at −20 °C. Thawed cell pellets were disrupted by sonication, and the debris was separated by centrifugation at 30,000 × *g* at 4 °C for 1 h. The resulting supernatant was decanted and applied to a pre-equilibrated HisTrap FF (GE Healthcare, 5 ml) at room temperature. Once supernatant was applied, the column was washed with 10 column volumes of 50 mM Tris-HCl, pH 7.5, 500 mM NaCl, 20 mM imidazole, and the protein was eluted in steps using 50 mM Tris-HCl, pH 7.5, 500 mM NaCl, 20–500 mM imidazole. The eluant was collected and fractionated, and the protein composition was assessed by SDS-PAGE. Fractions containing the PH domain were pooled and concentrated using a centrifugation filter device (Millipore) with a molecular weight cutoff of 10 kDa. The concentrated protein solution was applied to a pre-equilibrated Sephadex S75 (16/60) size exclusion chromatography column (GE Healthcare) at 4 °C. Size exclusion chromatography was performed using 20 mM Tris-HCl, pH 7.5, 200 mM NaCl, 0.5 mM Tris(2-carboxyethyl)phosphine or 1 mM dithio-

threitol. The eluant was monitored by absorbance at 280 nm and fractionated for collection. Fractions containing homogeneous protein were pooled and concentrated for crystallization. Recombinant kindlin-2 and kindlin-3 PH domains were expressed in *E. coli* Rosetta (pLysS/RARE) using standard isopropyl 1-thio-β-D-galactopyranoside induction procedures and purified analogously to recombinant kindlin-1 PH domain.

Protein Crystallization—Crystallization screening was performed using commercially available crystallization reagents by means of vapor diffusion methods. 100-nl sitting drops of protein solution (5–12 mg/ml in 20 mM Tris-HCl, pH 7.5, 200 mM NaCl, 0.5 mM Tris(2-carboxyethyl)phosphine) were diluted with an equal volume of crystallization solution. Sitting drops were equilibrated against 100 μl of crystallization reagent at room temperature and were duplicated for equilibration at 4 °C. Crystals appeared in several polyethylene glycol (PEG)-based conditions in 2–3 weeks at 4 °C only. A single condition (20% (w/v) PEG3350, 200 mM sodium phosphate) yielded the largest crystals and was optimized by stepwise dilution of the crystallization condition from 100% to 79% with sterile water with sterile water together with optimizing the protein:crystallization solution drop ratio. Optimal crystals grew within 16 days, with the largest crystals ~1 mm in the longest dimension. Crystals were cryo-protected with mother liquor supplemented with 25–30% (v/v) glycerol and directly frozen in liquid nitrogen before data collection.

Data Collection, Structural Determination, and Refinement—Diffraction data from a single native kindlin-1 PH domain crystal were collected at Diamond Light Source (Didcot, UK) on beamline IO3. Diffraction data were indexed and integrated using *iMOSFLM* (29) and were subsequently merged and scaled using the CCP4 program SCALA (30). The crystal form belongs to the C-centered orthorhombic space group $C222_1$ with unit cell dimensions $a = 45.7$Å, $b = 84.1$Å, $c = 95.9$Å, $\alpha = \beta = \gamma = 90°$ and possesses one molecule per asymmetric unit (solvent content of ~49% with a ~20-kDA protein, as determined by Matthews' coefficient). The structure of the kindlin-1 PH domain was solved by molecular replacement using PHASER (31) with the Protein Data Bank (PDB) coordinates at accession code 2YS3[4] as a search model. The model was converted to a poly-alanine chain in CHAINSAW (30) to reduce model bias. Separate molecular replacement calculations in PHASER were performed using individual models from the NMR ensemble. A single model yielding an optimal *Z*-score (RFZ = 6.3, TFZ = 6.9) and log likelihood gain (LLG = 59) was used. Phases calculated from this model were used for automatic model building in ARP/wARP (32). Model building in Coot (33) was continued from the map output by ARP/wARP, and the model was refined using a translation libration screw refinement protocol and individual B-factor refinement in Phenix (31). Translation libration screw (TLS) groups were determined using the TLS motion determination server (TLSMD) (34). Water molecules were added in Coot and updated during rounds of refinement in Phenix. The refinement resulted in an R_{free} and R_{work} of 21.3 and 18.2%, respectively. The crystal structure was validated using MolProbity (35) with 98.3% of the refined residues in favored regions and none in disallowed regions. The final model contains residues 369–497 (mouse *FERMT1* numbering). Weak electron density was observed for residues 382–388, which is why they were not built. The crystallographic data collection and refinement statistics are summarized in Table 1.

Structure Analysis—A representative selection of 32 PH domains, including kindlin-1, with diverse functions were selected from a list of structural homologues compiled using the protein structure database webserver DALI (36). Superimposition of all PH domains was performed using SHP (37). A single chain (A) was selected from structures containing more than one chain in the asymmetric unit and the first model only from NMR ensembles. In the case of multidomain structures, the PH domain was excised from the most complete molecule in the asymmetric unit. The phylogenetic tree was calculated using an evolutionary distance matrix (38). The tree representation was generated using the programs FITCH and DRAWTREE as part of the PHYLIP package (39). Structural alignments were inspected manually in Chimera (40) before the phylogenetic tree was constructed.

Molecular Dynamics Simulations—We used MODELLER (41) in combination with the MMTSB Toolset (42) to place the missing region in the crystal structure, which comprises residue numbers 382–388 with sequence Pro-Lys-Lys-Leu-Met-Leu-Lys. A total of 200 models were generated. These were clustered based on the conformations adopted by the flexible loop formed by residues 382–388. The top cluster was extracted on the basis of the average MODELLER score, and the highest scoring model from this cluster was used as a starting point for the MD simulations.

MD simulations were performed with GROMACS Version 4.0.5 (43) using both the united-atom GROMOS96 43al forcefield (44) and the all-atom OPLS-AA/L forcefield (45) with a time step of $\Delta t = 2$ fs. The protein was placed in a cubic box with sides of length 60 Å, and solvent molecules were subsequently added. The simple point charge (46) water model was used in conjunction with the GROMOS 43a1 forcefield, whereas the TIP4P (47) water model was used with the OPLS-AA/L forcefield. Chloride ions were added to neutralize the net charge of the system. Temperature was maintained at 310 K by coupling to a Berendsen thermostat (48) with a coupling constant of $\tau_T = 0.1$ ps. Pressure was kept constant at 1 atm using a Parrinello-Rahman barostat (49, 50) with isotropic pressure coupling, a coupling constant of $\tau_p = 1.0$ ps, and a compressibility of 4.6×10^{-5} bar^{-1}. Bond lengths and angles were constrained using the LINCS algorithm (51). Electrostatics interactions were treated with the particle mesh Ewald (52) method using a cutoff of 10 Å.

Molecular Docking—AutoDock Version 4.2 (53, 54) was used for ligand docking. The ligand structures used for molecular docking were extracted from high resolution x-ray crystal structures deposited in the PDB. The headgroups of six of the seven physiological phosphoinositide (PtdIns) isoforms were used in the docking calculations: Ins(1,3)P_2 (PDB code 1JOC) (55), Ins(1,4)P_2 (PDB code 1I9Z) (56), Ins(1,3,4)P_3 (PDB code 1Z2P) (57), Ins(1,3,5)P_3 (PDB code 1ZVR) (58), Ins(1,4,5)P_3 (PDB code 1MAI) (59), and Ins(1,3,4,5)P_4 (PDB code 1UNQ)

[4] H. Li, M. Sato, S. Koshiba, S. Watanabe, T. Harada, T. Kogawa, and S. Yokoyama, unpublished information.

(60). Although in total there are seven naturally occurring PtdIns isoforms in eukaryotic cells, to the best of our knowledge no structures with Ins(1,5)P_2 bound have yet been reported. Structures were prepared for docking by adding Gasteiger partial charges and ligand torsions using AutoDockTools. The protein was kept rigid, and grid maps were calculated using 80 × 80 × 80 grid points with a spacing of 0.375 Å. Grids were centered such that they encompassed the whole kindlin-1 PH domain.

The Lamarckian genetic algorithm was used for ligand conformational searching, and our docking parameters were based on those used in Ref. 61. For each run we performed 100 trial dockings with a population size of 300. Translation step ranges were 1.5 Å, and rotation step ranges were 35°. Elitism, mutation rate, cross-over rate, and local search rate were set to 1, 0.02, 0.8, and 0.06, respectively, with 25 million energy evaluations and 27,000 generations. Starting positions and conformations were randomized, and clusters were evaluated using a tolerance of 1.5 Å root mean square deviation (r.m.s.d.). To validate our docking results, we also performed blind dockings using SwissDock (62) using the accurate/default parameter preset (63). Ligands were converted to the SYBYL MOL2 format before docking using PRODRG (64).

Lipid Overlay Assay—PIP Strips™ (Echelon Biosciences Inc.) membranes were incubated with 1% (w/v) nonfat milk in PBS for 1 h at room temperature. This blocking solution was replaced with recombinant kindlin-1 PH domain or mutant PH domain (1.0 μg/ml in 1% (w/v) nonfat milk and PBS) and incubated for 2 h at room temperature. The protein solution was decanted, and the membrane was washed with PBS for 15 min for a total of 3 washes. The membrane was incubated with a mouse anti-penta-His antibody (1:2000 dilution) in 1% (w/v) nonfat milk in PBS for 1 h at room temperature. The primary antibody solution was discarded, and the membrane was washed as described earlier with PBS and 0.1% (v/v) Tween-20. The membrane was incubated with goat anti-mouse HRP-conjugated antibody in PBS with 1% (w/v) nonfat milk for 1 h at room temperature. The secondary antibody solution was discarded, and the membrane was washed as before. Subsequently, the membrane was incubated with Amersham Biosciences™ ECL™ Western blotting detection reagent (GE Healthcare) and then exposed to Amersham Biosciences™ Hyperfilm ECL™ (GE Healthcare) for variable times (30 s–20 min) at room temperature.

Surface Plasmon Resonance—A BIAcore CM5 chip was derivatized with streptavidin following the manufacturer's instructions, and by this means biotinylated inositol phosphate could be attached to the biosensor surface. Glo-PIPs were purchased from Echelon Biosciences as follows: PtdIns-(3)P (C-03B6a), PtdIns(5)P (C-05B6a), PtdIns(3,5)P_2 (C-35B6a), and PtdIns(3,4,5)P_3 (C-39B6a). After immobilization, the analytes (wild type PH domains of all three kindlins and the E416A mutant from kindlin-1) were applied at a flow rate of 10 μl/min for a total time of 6 min; dissociation time was set to 15 min. Experiments were run in both PBS and a HEPES-based buffer as reported elsewhere (10 mM HEPES, pH 7.5, 150 mM NaCl, 0.005% (v/v) Tween-20 and 3 mM EDTA) (24). Output sensograms were analyzed using BIAcore BIAanalysis software and Scrubber (BioLogic Software), which gave similar results, and by Scatchard analysis using ProFit software (Uetikon-am-See, CH).

RESULTS

The PH Domain Is Important for Kindlin-1-mediated Integrin Activation—A defining feature of kindlins is the insertion of a predicted PH domain within a loop of the kindlin F2 subdomain. To investigate the importance of the inserted PH domain in integrin activation, we generated a GFP-kindlin-1 expression construct that lacked the PH domain (kindlin-1ΔPH) and tested it in a well validated flow cytometric assay for αIIbβ3 integrin activation. As previously reported (5, 16, 27), when co-expressed with DsRed-tagged talin head, GFP-kindlin-1 enhanced activation of αIIbβ3 stably expressed in CHO cells (Fig. 1*A*). However, the ability of kindlin-1ΔPH to activate αIIbβ3 was significantly impaired compared with wild type kindlin-1. Kindlin-1ΔPH did nonetheless induce a small, but statistically significant increase in integrin activation compared with talin head alone (Fig. 1*A*). Additionally, the PH domain alone does not co-activate integrins (Fig. 1*C*). In all cases cells were gated to have comparable GFP fluorescence levels and fixed DsRed fluorescence ensuring that the impaired ability of kindlin-1ΔPH to activate αIIbβ3 was not due to altered kindlin or talin head expression levels. Furthermore, integrin activation was normalized to total surface αIIbβ3 integrin expression assessed in parallel by antibody staining. Western blotting confirmed that the GFP-kindlin-1, GFP-kindlin-1ΔPH, and GFP-kindlin-1 PH were of the expected size (Fig. 1, *B* and *D*). These data together with published data on kindlin-2 (3, 22, 24) show that the kindlin PH domain is important for kindlin-mediated integrin activation.

Overall Structure of Kindlin-1 Pleckstrin Homology Domain—To investigate the molecular basis of its function, amino acid residues corresponding to the PH domain (residues 356–509) of kindlin-1 were cloned, overexpressed, and purified from *E. coli*. Crystals of kindlin-1 PH domain were then generated, and their x-ray structure was solved by molecular replacement (see "Experimental Procedures" and Table 1).

The kindlin-1 PH domain structure is composed of 129 amino acids and exhibits an archetypal pleckstrin homology family fold at its core that is a partly collapsed seven-stranded β-barrel capped at one end by a C-terminal α-helix. The N-terminal half of the PH domain is composed of a four-stranded anti-parallel β-sheet (β1-β4), whereas the remaining three strands form a second anti-parallel β-sheet (β5-β7) that stacks nearly orthogonally against the first. This β-sandwich is filled with hydrophobic residues forming its core and is capped at one opening of the β-barrel (encircled by strands β1 and β7) by a predominantly hydrophobic C-terminal α-helix (α1). In PH domain folds, the helix that caps this opening of the β-barrel is typically amphipathic, with its hydrophobic residues buried in the core and polar residues exposed to the solvent (66). However, in the case of the kindlin-1 PH domain, the majority of this helix is hydrophobic, with hydrophobic residues facing into and away from the β-barrel (Fig. 2). This feature, which is conserved in all known kindlin protein PH domains, stabilizes the stacking of an additional C-terminal extension that is composed of a single amphipathic helix (α2) not found in other PH domains

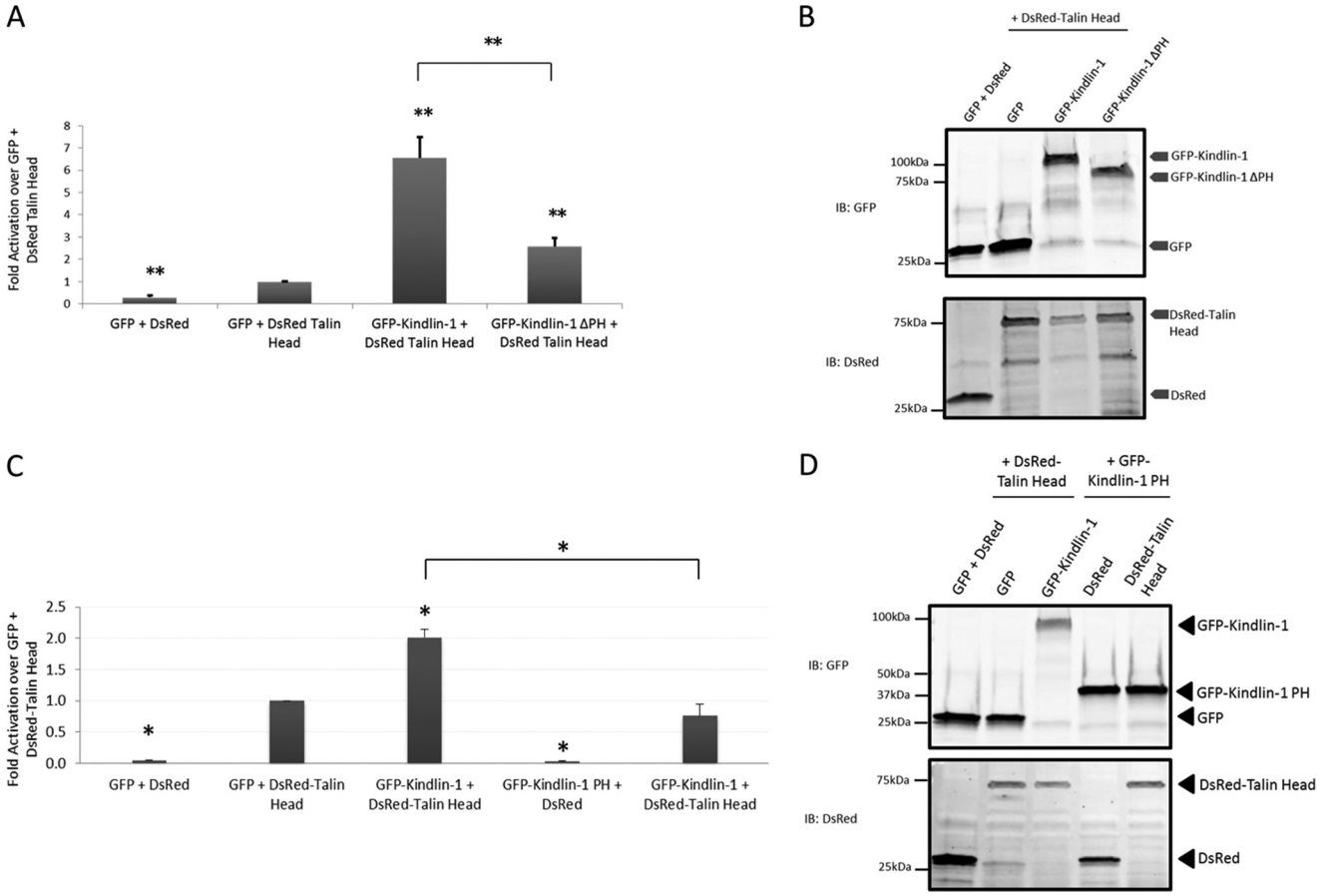

FIGURE 1. **Kindlin PH domain is important for kindlin-mediated co-activation of $\alpha IIb\beta 3$ integrins.** DsRed or DsRed-talin head and GFP-kindlin-1, GFP-kindlin-1 ΔPH, or GFP-kindlin-1 PH were transiently co-expressed in CHO cells stably expressing $\alpha IIb\beta 3$ integrins as indicated. *A* and *C*, activation indices were calculated for cells with similar amounts of DsRed and GFP mean fluorescence intensities (normalizing for total surface integrin levels) and expressed relative to GFP + DsRed-talin head. Results represent the means ± S.E. ($n \geq 3$). A two-tailed Student's *t* test was used to test for significant difference from GFP+ DsRed-talin head (**, *p* value <0.01; *, *p* value <0.02). GFP-kindlin-1 ΔPH was also significantly different from GFP-kindlin-1 (*p* value = 0.004). *B* and *D*, expression of the constructs was checked by lysing the cells and immunoblotting (*IB*) using anti-GFP (Rockland), Alexa 680 Fluor-coupled anti-goat (Invitrogen), anti-DsRed (Clontech), and anti-rabbit IgG IRDye800 conjugated (Rockland).

(Fig. 2). The interconnecting loop that lies between the $\alpha 1$ and $\alpha 2$ helices is highly conserved across all kindlin isoforms (see Fig. 3). An invariant methionine (Met^{477}) within the $\alpha 1$-$\alpha 2$ loop is involved in the stabilization of the $\alpha 1$-$\alpha 2$ hydrophobic interactions (see Fig. 2), where the methionine side chain interacts with a tyrosine (Tyr^{482}) side chain from $\alpha 2$ and a leucine (Leu^{373}) from the $\beta 1$ strand. Sequence alignment between mammalian kindlin isoforms and UNC-112, the sole kindlin protein from *Caenorhabditis elegans* indicates that those amino acids responsible for the hydrophobic properties of $\alpha 1$ and the amphipathicity of $\alpha 2$ that mediate the $\alpha 1/\alpha 2$ helix packing are highly conserved alongside the $\alpha 1/\alpha 2$ loop invariant across all species (Fig. 3). This suggests that this C-terminal extension is an integral part of the PH domain fold found in kindlins.

Structural and Molecular Dynamic Simulation Analysis Reveal That Ligand Binding Is Dictated by a Kindlin-1-specific Salt Bridge—Pleckstrin homology domains were first identified as phosphoinositide binding modules that target proteins to the membrane in a phosphoinositide-dependent manner (67). The phosphoinositide binding affinity/specificity is governed by three variable loops (VL1, -2, and -3) that crown the open end of the β-barrel ($\beta 1/\beta 2$ (VL1), $\beta 3/\beta 4$ (VL2), and $\beta 6/\beta 7$ (VL3) loops) (68). The $\beta 1/\beta 2$ loop is disordered in the kindlin-1 crystal structure so that very weak electron density corresponds to this region, suggesting that it has significant conformational flexibility. Additionally, the $\beta 3/\beta 4$ loop in kindlin-1 forms a small single-turn helix, denoted here as α' and similar to the PH domains of β-spectrin (69) and protein kinase B (PKB/Akt) (70). In the canonical PH domain the ligand would be expected to bind in the central binding pocket, although examples of PH domains with non-canonical PtdIns binding sites have been reported (71). In an effort to identify a putative lipid binding site, we performed molecular docking of the headgroups of six different PtdIns species to the kindlin-1 PH domain using AutoDock. Given the importance of the variable loops in ligand binding (68), before conducting the *in silico* docking experiments, the missing loop of the crystal structure was modeled using MODELLER (see "Experimental Procedures"). After modeling these residues, we conducted MD simulations of the kindlin-1 PH domain.

The crystal structure revealed a salt bridge between arginine 380 and glutamate 416 that traverses the open end of the β-barrel potentially occluding the canonical binding site (Fig. 2*B*). The variation in the spacing between Arg^{380} and Glu^{416} over the lifetime of the simulation is shown in Fig. 4*A* alongside

TABLE 1

X-ray data collection and structure determination

R_{work} and R_{free} were calculated from working and test set reflections.

Data collection and refinement statistics	
Space group	$C222_1$
Unit cell (Å, °)	$a = 45.29$, $b = 82.78$, $c = 95.99$, $\alpha = \beta = \gamma = 90$
Resolution[a] (Å)	41.4-2.1 (2.21-2.1)
Completeness (%)	95.4 (95.2)
Redundancy	7.0 (7.3)
$I/\sigma I$	13.7 (3.5)
R_{merge}[b]	0.083 (0.565)
$R_{p.i.m}$[c]	0.223
Average Wilson B-factor (Å^2)	32.2
Model and refinement	
Resolution (Å)	40-2.1 (2.4-2.1)
Unique reflections	10,324 (1,478)
R_{work}	0.1821
R_{free} (using 5% of reflections)	0.2131
Model contents	
Residues	370-496
Waters	49
Ligands	1 (glycerol)
Total number atoms	1,040
Average B-factor (Å^2)	
Protein/water	42.4/45.4
Glycerol	79.5
r.m.s.d. from ideal	
Bond lengths (Å)	0.008
Angles (°)	1.011
Ramachandran	
Favored (%)	95.3
Allowed (%)	3.7
Generously allowed (%)	0.9
Disallowed (%)	0.0

[a] Values in parentheses account for the highest resolution shell.
[b] $R_{merge} = \Sigma|I_o - I|/\Sigma I_o$.
[c] $R_{p.i.m.} = \Sigma_{hkl}[1/N-1]^{1/2}\Sigma_i|I_i(hkl) - \overline{I(hkl)}|/\Sigma_{hkl}\Sigma_i I_i(hkl)$.

images of the PH domain in "closed" and "open" states. Interestingly, although this salt bridge was typically preserved during the simulations, it switched transiently to a conformation involving an alternative salt bridge interaction Arg^{380}–Glu^{450} that leaves the binding pocket exposed. This transition between a partially occluded state and an open state was apparent in simulations using both the GROMOS96 43a1 forcefield and the OPLS-AA/L forcefield. The r.m.s.d. and root mean square fluctuation of the Cα atoms over the course of the simulation trajectories are shown in Fig. 4*B*. The Cα r.m.s.d. indicated that the protein experienced little conformational drift over a period of 100 ns. The Cα root mean square fluctuation suggested that of the three loops flanking the open end of the β-barrel, the $\beta1/\beta2$ loop appears to be the most flexible.

To begin modeling ligand binding, we first extracted a representative conformation of the kindlin-1 PH domain from the MD simulations in which the Arg^{380}–Glu^{416} salt bridge remained intact. However, when molecular docking was performed using this partially occluded state, the results were generally poor. Clustering the conformations resulted in a large array of small, spatially separated clusters, and little consensus emerged as to the location of any possible binding site. Fig. 4*C* shows the results from the docking runs using Ins(1,3,4,5)P_4 (equivalent to the headgroup of PtdIns(3,4,5)P_3). Indeed, even when the number of energy evaluations was increased by a factor of 500 to 10 billion, a likely binding site failed to emerge (data not shown). In the absence of a predicted binding site, we turned to the alternative open conformation observed in the MD simulations. Molecular docking using this open conformation extracted from the simulations led to improved results. Analysis produced a smaller number of larger clusters, and most of the docking runs placed the ligand in or near the central cavity (Fig. 4*C*). Docking using the open conformation rather than the occluded conformation significantly reduced the number of conformational clusters and multimember clusters. This higher level of consensus resulted in a reasonably consistent prediction of a putative binding site for all six PtdIns headgroups, lined by Arg^{380}, Lys^{382}, Lys^{390}, and Asn^{449} (data not shown). Performing similar docking runs using another docking program (SwissDock) yielded qualitatively similar results (data not shown).

This effect was even more pronounced when performing docking runs with the E416A mutant, which is predicted to be a permanently opened state. It appears that PtdIns binding is enhanced in the E416A mutant for two reasons; (i) the Arg^{380}–Glu^{416} salt bridge, which otherwise blocks the entrance to the binding pocket, is broken, and (ii) the sentry glutamate residue, Glu^{416}, is replaced by an alanine in this open state, which further increases the accessibility of the binding site for negatively charged lipid headgroups. This stepwise enhancement of PtdIns binding is confirmed by the estimated free energies of binding predicted by AutoDock, which suggest that docking to the E416A mutant (open) PH domain is more favorable than docking to the wild type (open), which in turn is an improvement over the wild type (closed) PH domain. In general, this trend was observed for all six PtdIns species, and the more favorable binding energies were accompanied by an improved level of clustering (Fig. 4*D*).

In Vitro Measurement of Inositol Phosphate Binding—To assess the ligand binding affinity of the kindlin-1 PH domain for lipid species we first made use of a lipid overlay assay (dot-blot) approach and found PH domain binding to PtdIns(3)P, PtdIns(4)P, and PtdIns(5)P but not to diphosphorylated inositides (Fig. 5*A*). The E416A mutant also bound to the PtdIns monophosphates but additionally to PtdIns(3,5)P_2 (Fig. 5*A*). We followed this up with a dot-blot in which a series of different PtdIns concentrations was presented and found that this supported the initial impression that wild type kindlin-1 PH domain binds to monophosphorylated PtdInsPs, whereas the mutant form binds more strongly to them and also recognizes PtdIns(3,5)P_2 (although not PtdIns(4,5)P_2 or PtdIns(3,4,5)P_3) (Fig. 5*A*). These data suggest that binding to PtsInsP species is enhanced by the E416A mutation, in agreement with the MD results reported above. However, it has been reported elsewhere (24) using surface plasmon resonance (SPR) that the wild type kindlin-2 PH domain does bind PtdIns(4,5)P_2 and PtdIns(3,4,5)P_3, so we next carried out similar experiments ourselves. We immobilized mono-, di-, and triphosphorylated inositol species on a BIAcore chip surface via biotin-streptavidin coupling and measured the binding of wild type and mutant kindlin-1 PH domains and the PH domains of kindlins 2 and 3 (see "Experimental Procedures"). We ran SPR experiments using both the HEPES buffer used elsewhere (24) and PBS. In contrast to the dot-blot data, we could detect no interaction between either form of the kindlin-1 PH domain and monophosphorylated species (Ins(3)P or Ins(5)P) in either Tris, PBS, or HEPES buffer (data not shown). The highest affinity interac-

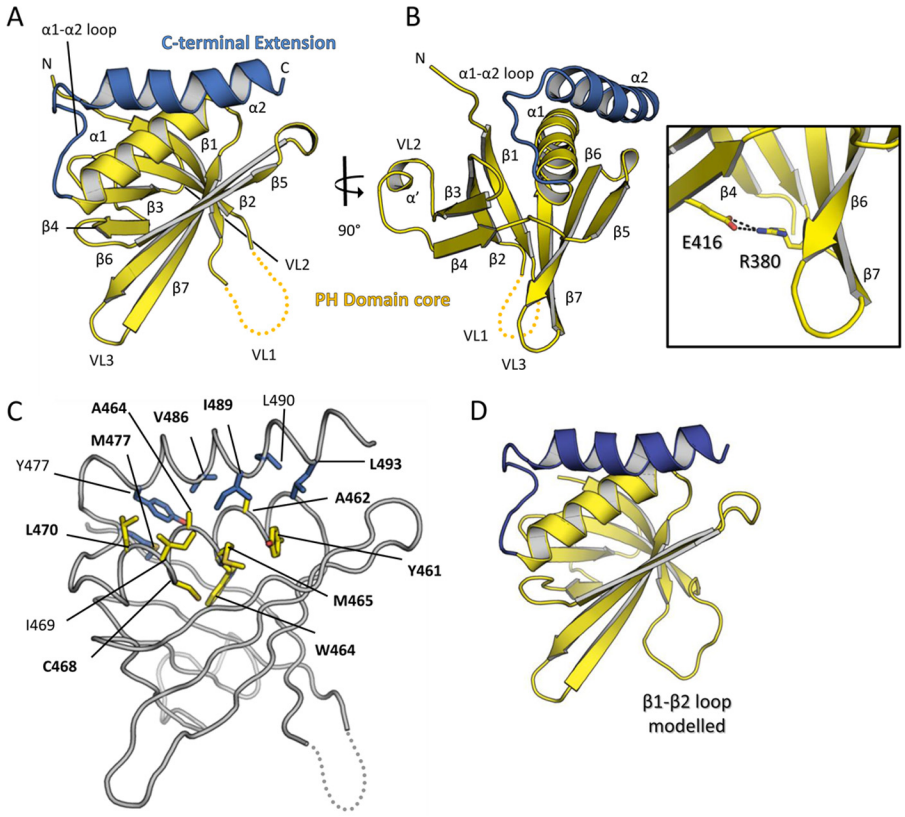

FIGURE 2. **Structure of kindlin-1 pleckstrin homology domain.** *A*, the kindlin-1 PH domain is composed of a core seven-stranded β-barrel (β1-β7) capped with two α-helices (α1-α2). The open end of the β-barrel is decorated with variable loops (*VL*), with VL2 (β3-β4 loop) forming a single-turn helix. The core archetypal PH domain fold is rendered in *yellow*, with the additional C-terminal extension α-helix, specifically found in kindlin proteins, rendered in *blue*. *B*, descriptions are as in *A* but rotated 90° to show the β-barrel fold together with the variable loop regions. To the right a close-up of the kindlin-1 PH domain pocket-spanning salt bridge is shown. *C*, shown are hydrophobic side chains, which stabilize the stacking of the α1 and α2. Hydrophobic residues contributing to the core of stacking helices are shown as *sticks*. Residues are labeled according to mouse full-length kindlin-1 numbering (UniProt accession code P59113) and those in bold indicate invariant residues conserved across the kindlin family in all species. *D*, the β1-β2 loop is disordered in the kindlin-1 PH crystal structure (*panel C*); in this schematic representation of the structure, it is shown modeled in. All panels were rendered in PyMol.

tions we did find were between the PH domains and $Ins(3,4,5)P_3$, and these data are shown in Fig. 5, *B* and *C*, analyzed both by direct fitting to the binding data and Scatchard plot. As listed in Table 2, the affinities of binding in HEPES were between K_D ~80 and 200 μM. The measured affinity of kindlin-2 PH domain is ~60× lower than reported elsewhere (24) (see "Discussion") despite our use of the same inositol phosphate species and buffer. The affinities of binding in PBS (Table 3) showed a similar range of K_D values to the HEPES conditions for $Ins(3,4,5)P_3$; the diphosphate tested under the same conditions had greatly reduced affinity (K_D ~500 to ~2000 μM; the diphosphate data were not amenable to Scatchard analysis). The pattern of a much-enhanced affinity for $Ins(3,4,5)P_3$ over $Ins(3,5)P_2$ is in agreement with data reported elsewhere that showed the same preference (24). However, the most interesting observation made is the significant improvement in affinity for the triphosphorylated species in HEPES found for the E416A mutant kindlin-1 PH domain compared with the wild type. This result supports the MD analysis suggesting that the E416A mutation would open up the domain binding pocket. Curiously, the wild type kindlin-1 and -2 PH domains showed a higher affinity in PBS compared with HEPES, and the kindlin-3 PH domain showed unaltered affinity, but the affinity of the kindlin-1 mutant was lower than the wild type in PBS when it was higher in HEPES. We discuss this further below. However, collectively, the data we present on ligand binding by kindlin-1 PH domain suggest that PtdInsPs may not be its native ligands but perhaps some other phosphorylated species; the same may be true for kindlin-3. To evaluate this possibility, further we undertook a structural comparison with other PH domain structures.

Structural Comparison of Kindlin-1 PH and Other PH Domains—A structural similarity search using the kindlin-1 PH domain in DALI (36) indicated, not surprisingly, that it is similar to other PH domains and phosphotyrosine binding domains, with a Z score range of 17.2–4.9 for >500 structures. The corresponding r.m.s.d. values for these aligned structures ranged from 1.8 to 4.2 Å using 60–124 Cα atoms with pairwise sequence identities ranging from 6 to 26%. Although we found a lower affinity of binding of the kindlin-2 PH domain to $Ins(3,4,5)P_3$ than that reported (24), the same paper described its solution structure in complex with inositol 1,3,4,5-tetrakisphosphate. This suggests that kindlin-2 is localized to the plasma membrane in a phosphatidylinositol 3-kinase product-dependent manner via its PH domain. Given the high level of sequence homology between the kindlin isoforms, their PtdInsP recognition modes might have been conserved so that all kindlins would be localized to the plasma membrane in a similar manner. Our binding data (above) show this is not the case, and a structural comparison between the kindlin-1 PH

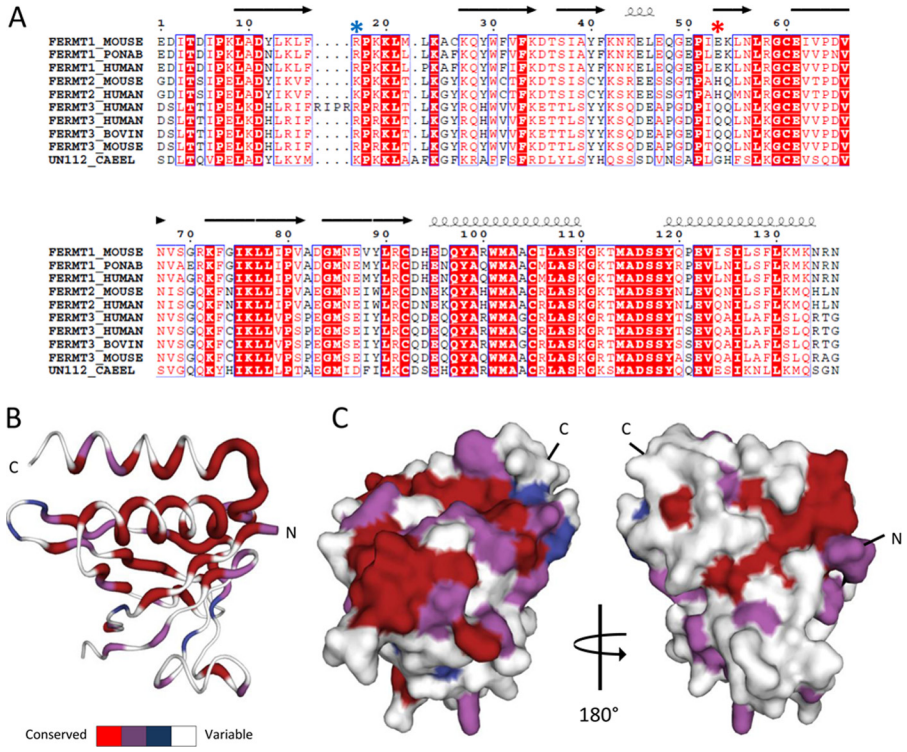

FIGURE 3. **Structure-based sequence alignment and projected conservation of kindlin pleckstrin homology domains.** *A*, ClustalW multiple sequence alignment of the kindlin-1 PH domain with the kindlin-1 crystal structure secondary structure is shown *above* with labeling analogous to Fig. 2. Invariant residues are *shaded in red boxes*, with residues that are conserved colored *red*, and variable residues shown in *black*. Multiple sequence alignment was prepared using ClustalW (65) and secondary structure superimposition prepared using ESPript (81). The sequences used are as follows: kindlin-1 of mouse (UniProt accession code P59113), orangutan (UniProt accession code Q5R8M5), and human (UniProt accession code Q9BQL6); kindlin-2 of mouse (UniProt accession code Q8CIB5) and human (UniProt accession code Q96AC1); kindlin-3 of mouse (UniProt accession code Q8K1B8), human isoform I (long) (UniProt Accession code Q86UX7–1), human isoform II (short) (UniProt Accession code Q86UX7–2), and cow (UniProt accession code Q32LP0); Unc-112 of the nematode worm (UniProt accession code Q18685). The positions of kindlin-1 Arg^{380} and Glu^{416} are marked by *blue* and *red asterisks*, respectively, to show that their salt bridge is unique to that kindlin isoform. *B*, kindlin PH domain sequence conservation is mapped onto a three-dimensional structure of kindlin-1 PH domain. Sequence conservation is shown with invariant residues colored *red*, highly conserved rendered *purple*, semi-conserved rendered *blue*, and variable rendered *white*. *C*, kindlin PH domain sequence conservation is projected onto a surface representation of kindlin-1 PH domain. Amino acid conservation is rendered as in *B*. Structural representation of sequence conservation was performed using ESPript (81) and rendered in PyMol.

domain and the kindlin-2 PH domains suggests several key structural explanations.

Within the kindlin-2 PH domain, the soluble headgroup of PtdIns(3,4,5)P_3 is bound in the canonical binding site at the open end of the β-barrel. Here, the 3-phosphate of the inositide is contacted by side chains; Lys^{383}, Lys^{393}, His^{419}, and Tyr^{395} (24). Sequence alignment suggests synonymous substitution of a lysine 383 in kindlin-2 with a conserved arginine in kindlin-1 (Arg^{380}), and in the apo form of kindlin-2 PH domain the two residues occupy equivalent positions (Fig. 6) (72). However, in the crystal structure of the kindlin-1 PH domain the Arg^{380}–Glu^{416} salt bridge across the open end of the β-barrel occludes the binding site; in the kindlin-2 Apo structure the Glu^{416} is replaced by His^{419}, producing an open pocket where kindlin-1 PH domain has a closed one, and the open pocket undergoes substantial deformation on binding to Ins(3,4,5)P_3 (Fig. 6). The structures are consistent with the *in silico* docking experiments and BIAcore studies; removal of the kindlin-1 PH domain salt bridge results in a larger binding pocket able to admit more substantially phosphorylated inositides and displaying a higher apparent affinity for them. The conservation of the salt bridge residues only in kindlin-1 across the species listed in Fig. 3 and the full range of other available sequences suggest an isoform-specific function. In further support of the idea that the kindlin PH domains have been selected distinctly for their ligand binding and, as discussed above, the basic His^{419} seems to be important for Ins(3,4,5)P_3 binding in the kindlin-2 complex structure, particularly at the 3- position of the inositol ring, and of course is equivalent to the acidic Glu^{416} in kindlin-1.

Comparing the kindlin-2 PH domains in apo and Ins(3,4,5)P_3-bound states shows that a dramatic conformational switch accompanies ligand binding to generate an induced fit and how bonding interactions throughout the domain sequence may influence the strength of interaction on ligand recognition (24, 72). In the kindlin-1 PH domain the salt bridge constriction of the binding pocket is augmented by hydrophobic stacking interactions. For example, Tyr^{403}, Tyr^{392}, and Phe^{394} make the putative kindlin-1 PtdInsP binding site very shallow and alter its electrostatic characteristics due to the tyrosine hydroxyl moieties (Fig. 6). These bulky aromatic side chains will prevent basic residues also present in the binding site from interacting with negatively charged lipids. Thus, the structural data for the kindlin-1 PH domain show that the binding pocket is occluded and suggest the reason why kindlin-1 does not bind to inositol phosphates with high affinity, consistent with MD simulation docking experiments and *in vitro* PtdInsP surface plasmon resonance analysis.

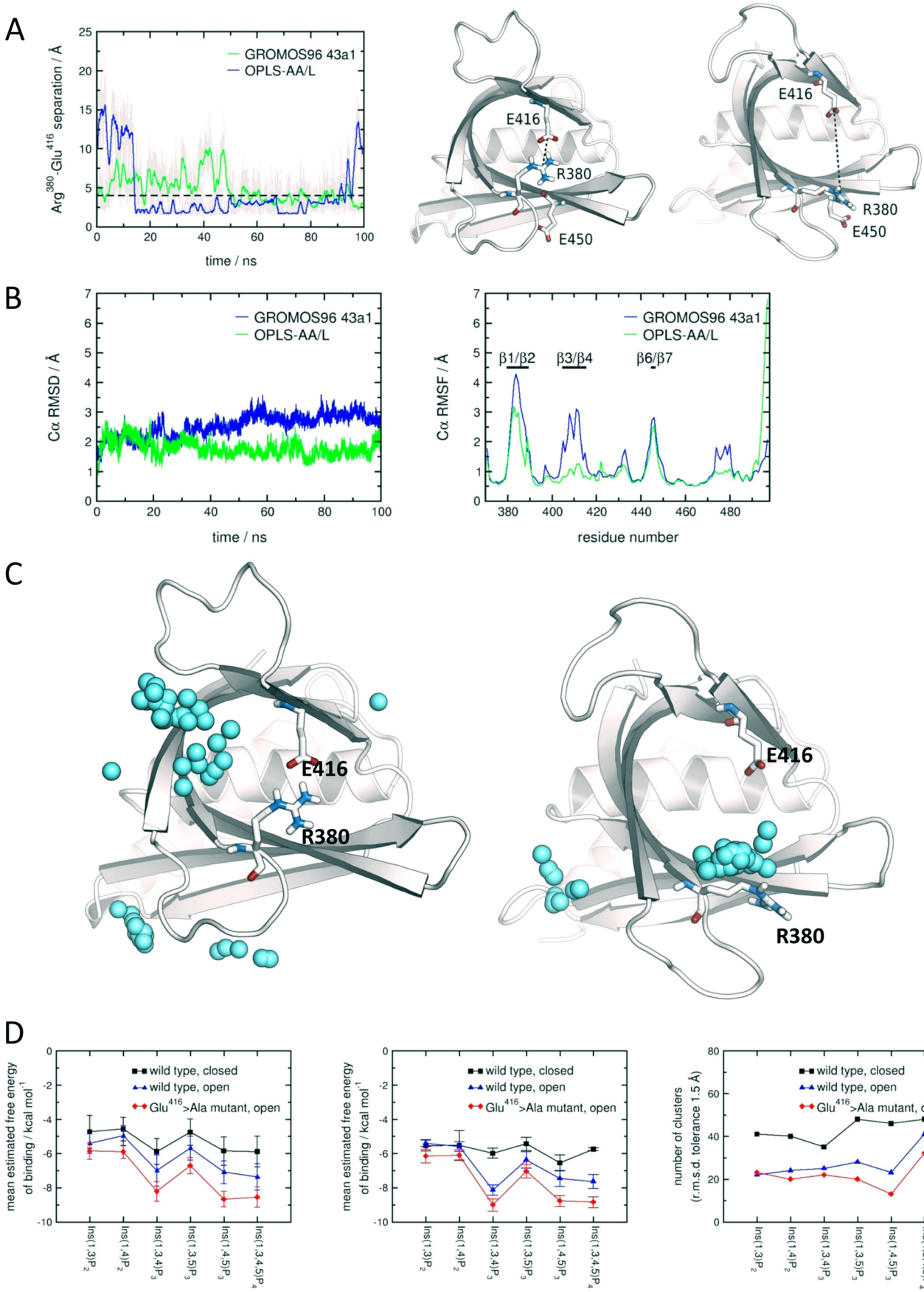
A
GROMOS96 43a1
OPLS-AA/L
Arg380-Glu416 separation / Å
time / ns
E416
R380
E450
B
GROMOS96 43a1
OPLS-AA/L
Cα RMSD / Å
time / ns
β1/β2
β3/β4
β6/β7
Cα RMSF / Å
residue number
C
E416
R380
D
wild type, closed
wild type, open
Glu416>Ala mutant, open
mean estimated free energy of binding / kcal mol-1
number of clusters (r.m.s.d. tolerance 1.5 Å)
Ins(1,3)P2
Ins(1,4)P2
Ins(1,3,4)P3
Ins(1,3,5)P3
Ins(1,4,5)P3
Ins(1,3,4,5)P4

Phylogenetic Relationships of Kindlin PH Domains—Because structural comparisons with other kindlins suggest the kindlin-1 PH domain has little capacity to bind to PtdInsPs, a wider structure comparison and analysis may provide a clearer idea as to its functional role. Given the diverse nature of PH domain function despite a common fold (68), we constructed a structural phylogeny using an all-pairs, pairwise structural superimposition of the kindlin-1 PH domain and a large number of PH domain structures from the PDB (38) to investigate evolutionary relationships between them (Fig. 7). PH domains known to bind to inositol phosphate lipid ligands cluster together. Interestingly, murine T-lymphoma invasion and metastasis-1 (Tiam1) PH domain is positioned close to β-spectrin from the same species, both of which share a noncanonical modality of binding to PtdInsP ligands (71, 73) and are positioned away from those PH domains that bind to PtdInsPs in a canonical mode, such as Grp1 (74), from the same species. Furthermore, human ArhGAP9 PH domain, also considered β-spectrin-like in its mode of binding PtdInsP (71), branches from the same common scaffold as Tiam1 and β-spectrin. Moreover, those PH domains that predominantly bind directly to Rho family G-protein ligands, such as intersectin and Dbs (75), also cluster with structural paralogues positioned close to one another, with orthologous structures branching from the same common scaffold. Conversely, Tiam1, the PH domain of which is positioned along with β-spectrin-like PH domains, also binds to the Rho GTPase, Rac1 (76). However, the PH domain of Tiam1 in this case does not contact the GTPase directly (77). It is quite apparent that a large number of PH domains are closely associated, thus dividing the tree in half at its root (see Fig. 7). Those closely related PH domains are known to bind to phophatidylinositol phosphate ligands, and on closer inspection it seems that the vast majority possess micromolar (μM) dissociation constants (*e.g.* Akt/PKB, $K_D = 1$ μM (78); PEPP1, $K_D = 0.32$ μM (79)) with some PH domains with nanomolar affinity (*e.g.* Bruton's tyrosine kinase (BTK), $K_D = 0.04$ μM (80); FAPP1 (four-phosphate-adaptor protein 1), $K_D = 0.04$ μM (79)) within this grouping (some of those PH domains with nanomolar affinity were clustered, but this is more than likely an artifact primarily due to their all being from *Homo sapiens* and, therefore, structural paralogues).

Among those PH domains in the less related, opposing half of the phylogeny, a small number of proteins possess μM dissociation constants for inositol phosphates, but the majority prefer protein ligands. According to this structural analysis, kindlin-1 is closely related, as expected, to kindlin-2 and -3 PH domains and is unexpectedly structurally related to oxysterol-binding protein-related protein 11 (OSBP11), sharing a common ancestral protein module. The canonical PtdIns binding PH domains cluster together, and kindlin-1 is clearly evolutionarily related to these modules, but the fact that it does not cluster with other PtdIns binders suggests a distinct, but as yet unidentified function, as does its failure to bind inositol phosphates tightly (see above). A calculated projection of electrostatic surface potential on the kindlin-1 PH domain crystal structure (Fig. 8*A*) and of the structure with a modeled β1-β2 loop (see "Experimental Procedures" (Fig. 8*B*)) compared with other kindlin isoform PH domains, a non-canonical PtdIns binding PH domain (β-spectrin) and a canonical PtdIns binding PH domain (pleckstrin), reveals a surface charge distribution reminiscent of a non-canonical binding modality, although the kindlin-1 PH domain does not possess the relevant side chains to coordinate PtdInsP ligands in the way that β-spectrin does; on the other hand, it does not possess a negatively charged cavity at the opening of the β-barrel similar to that found in kindlins 2 and 3 either (Fig. 8).

DISCUSSION

Kindlin-1 is a co-activator of integrins alongside talin, enriched in epidermal keratinocytes among other tissues (1, 10). A variety of pathological conditions help to underscore the importance of all three mammalian kindlins in the fundamental biology of cell adhesion (1). Kindlins are distinguished from talin by two features; they are the absence of a C-terminal rod domain and the presence of an additional PH domain interposed between the N- and C-terminal halves of the FERM F2 subdomain (27). The pleckstrin homology domain is the 11th most common module in the human genome (66) and despite a common scaffold is diverse in function.

In the work reported here we have shown that the kindlin PH domain is important for kindlin-1-mediated integrin activation. The determination of the crystal structure of the kindlin-1 PH domain has, like the structures of kindlin-2 PH domain (24, 72), revealed a C-terminal helix not present in other reported PH modules that is integral to the fold. By making use of *in silico* molecular dynamics simulation and ligand docking techniques with the determined structure we have shown that a novel kind-

FIGURE 4. **MD simulations of the kindlin-1 PH domain.** *A*, *left*, shown is separation between the charged groups of Arg^{380} and Glu^{416}, which together form a salt bridge in the crystal structure that appears to partially occlude the putative lipid binding cavity. Running averages taken every 100 ps show the transient breaking of the salt bridge over the course of both the GROMOS96 43a1 simulation (*green*) and the OPLS-AA/L simulation (*blue*). The *dashed line* at 4 Å indicates the separation at which the salt bridge is considered to be formed/broken following the published definition (82). *Center*, shown is a simulation snapshot of the occluded conformation used for docking, with the Arg^{380}–Glu^{416} salt bridge intact. *Right*, shown is a simulation snapshot of the open conformation used for docking, with the Arg^{380}–Glu^{416} salt bridge now broken and replaced by an alternative Arg^{380}-Glu^{450} salt bridge, leaving the binding pocket exposed. *B*, shown are conformational dynamics of the kindlin-1 PH domain during the MD simulations. *Left*, Cα r.m.s.d. was calculated as a function of time over the MD simulations using the GROMOS96 43a1 forcefield (*green*) and the OPLS-AA/L forcefield (*blue*). *Right*, shown is Cα root mean square fluctuation calculated for each residue over the course of the MD simulations. *C*, molecular docking of Ins(1,3,4,5)P_4 (equivalent to the headgroup of PtdIns(3,4,5)P_3) using AutoDock. *Left*, centers of mass of the ligand clusters when docking to the occluded conformation are shown. Based on a cluster tolerance of 1.5 Å r.m.s.d. from 100 docking runs, there were a total of 48 distinct conformational clusters, of which 22 were multimember clusters. *Right*, shown are centers of mass of the ligand clusters when docking to the open conformation. In this case, from 100 docking runs there were now 41 distinct conformational clusters, of which only 14 had multiple members. *D*, shown are estimated free energies of binding and number of clusters using AutoDock. *Left*, shown is mean estimated free energy of binding for all 100 docking runs using AutoDock for each of the six PtdIns species. Results are shown for docking to the wild type (*closed*) PH domain (*black squares*), wild type PH domain (*blue triangles*), and E416A mutant PH domain (*red diamonds*). *Error bars* are ±1 S.D. Lines are guides for the eye. A more negative value is indicative of more favorable binding. *Center*, mean estimated free energy of binding for the members of the largest cluster after docking is based on a cluster tolerance of 1.5 Å r.m.s.d. Similar trends to those in the left hand panel are observed. *Right*, number of clusters after 100 docking runs for each case is shown. A lower number of clusters suggests a greater degree of consensus as to the location of the binding site.

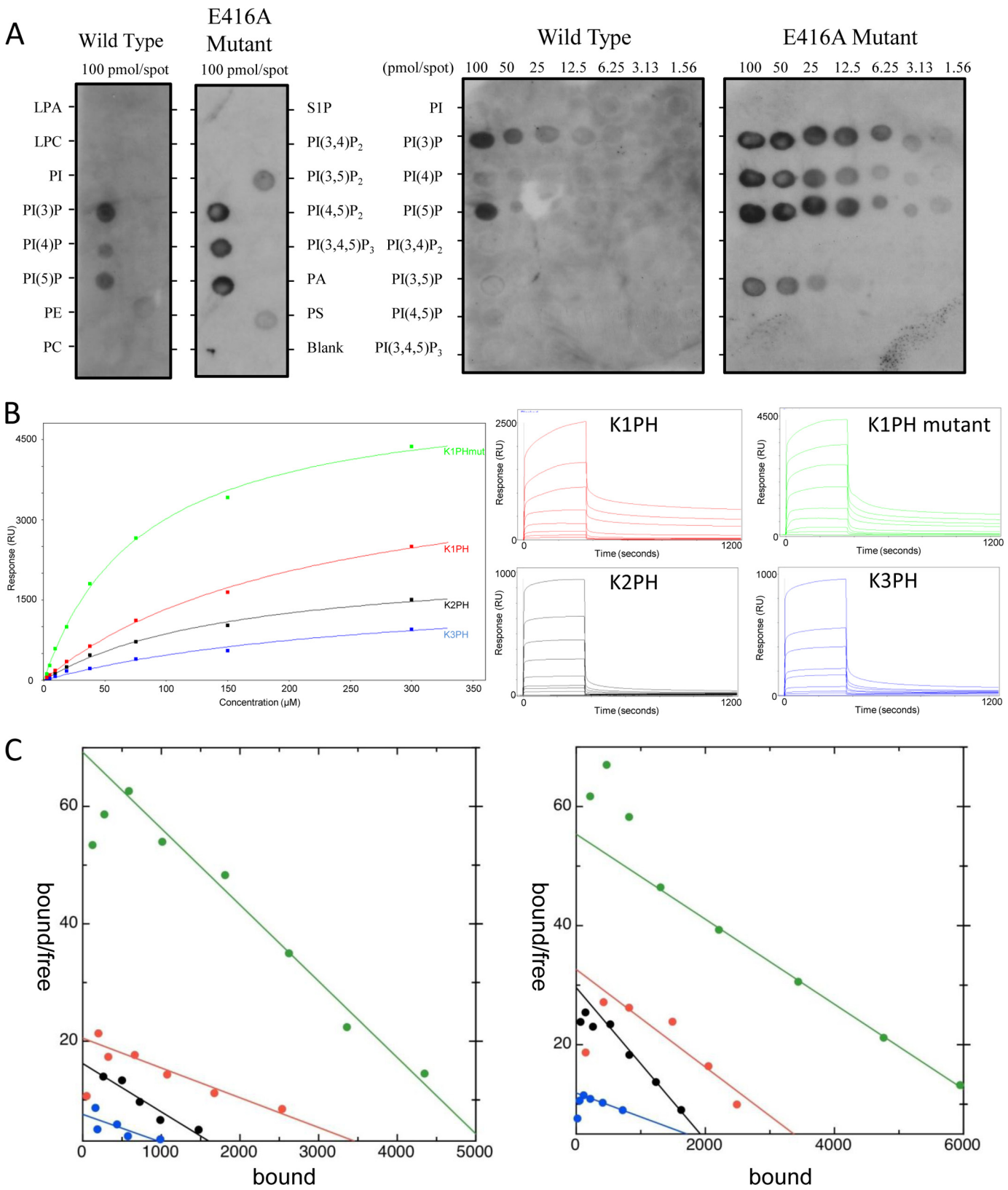

FIGURE 5. **Kindlin PH domain binding to inositol phosphates.** *A*, shown is lipid overlay assay (dot-blot) of the kindlin-1 PH domain and E416A mutant. *LPA*, lysophosphatidic Acid; *LPC*, lysophosphophocholine; *PI*, phosphatidylinsoitol; *PE*, phosphatidylethanolamine; *PC*, phosphatidylcholine; *S1P*, sphingosine 1-phosphate; *PA*, phosphatidic acid; *PS*, phosphatidylserine. *B* and *C*, shown is SPR analysis of kindlins 1–3 binding to Ins(3,4,5)P_3. *B*, shown are direct responses in HEPES buffer. Kindlin-1 (*red*), kindlin-1 E416A mutant (*green*), kindlin-2 (*black*), and kindlin-3 (*blue*) PH domains were analyzed by binding curve fit using Scrubber software. The K_D values determined are listed in Table 2. The binding responses of the four kindlin PH domains are shown on the *right* according to the same color scheme. *C*, Scatchard analysis of kindlin PH domain binding to Ins(3,4,5)P_3 is shown. *Left*, in HEPES buffer as used elsewhere (24), *i.e.* the data reported in *panel A*. The K_D values determined as −1/slope are listed in Table 2. *Right*, in PBS; for K_D values see Table 3. Colors are as in *panel A*.

TABLE 2

Affinity for Ins(3,4,5)P_3 in HEPES buffer, K_D values in μM

See Fig. 5 for data relating to this table. Note the agreement between binding curve and Scatchard analyses.

Protein domain	Binding curve fit	Scatchard analysis
K1PH	224	196
K1PH mutant	80.6	77
K2PH	159	121
K3PH	284	211

TABLE 3

Affinity for Ins(3,5)P_2 and Ins(3,4,5)P_3 in PBS, K_D values in μM

See Fig. 5 for data relating to this Table. Note the agreement between binding curve and Scatchard analyses.

Protein domain	Ins(3,4,5)P_3 binding curve fit	Ins(3,4,5)P3 Scatchard	Ins(3,5)P2 Binding curve fit
K1PH	98.5	122	1660
K1PH mutant	137.3	140	2370
K2PH	85.7	78.2	950
K3PH	262	248.8	530

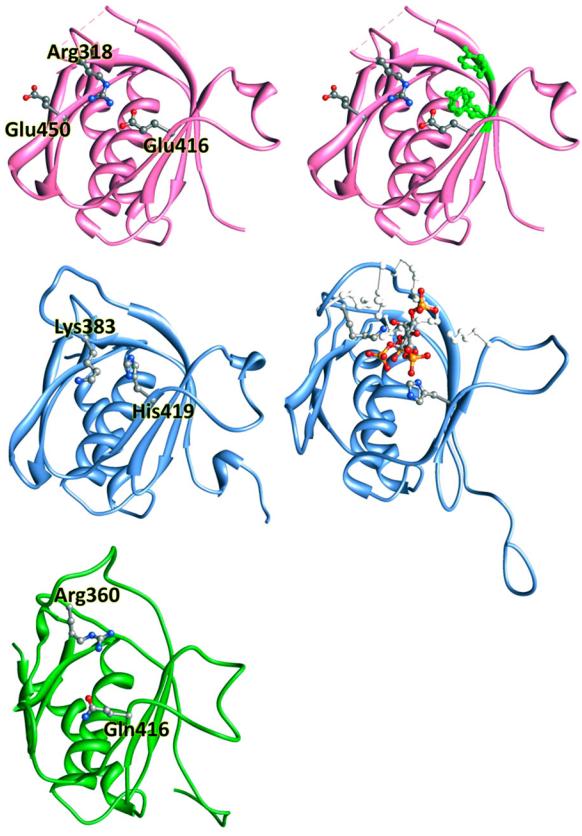

FIGURE 6. **Comparison of kindlin PH domain structures.** The kindlin-1 PH domain structure reported here (*top*; with aromatic residues projecting into the binding pocket shown in *green on the right*), the apo (*left*) (72) and Ins(1,3,4,5)P_4-bound NMR structure (equivalent to Ins(3,4,5)P_3 binding physiologically) (*right*) (24) of the kindlin-2 PH domain (*middle*), and the kindlin-3 PH domain structure (*bottom*) (PDB ID 2YS3). The residues involved in the native salt bridge are shown for the kindlin-1 structure, and the structural equivalents for the other PH domain; the alternative salt bridge partner Glu^{450} is also shown for kindlin-1 and in the InsP-bound structure of the kindlin-2 domain, the interacting side chains other than His^{419} and Lys^{383} are shown in *white*.

lin-1-specific salt bridge in the crystal structure prevails in the simulation and occludes the putative lipid binding site. Further analysis suggests that this salt bridge restricts the binding of secondary messenger lipid head groups, limiting its recognition of and its affinity for PtdInsP species. The kindlin-1 PH domain shows a lower affinity for phosphoinositides than the kindlin-2 PH domain in our hands, but the apparent affinity of the latter is substantially lower than that reported elsewhere (24). Removal of the kindlin-1 PH domain salt bridge increases the affinity of the protein for Ins(3,4,5)P_3 markedly over that of the kindlin-2 domain even but only in a HEPES buffer. In contrast, phosphate buffer reduces the affinity. These data in themselves suggest a nonspecific interaction between the kindlin-1 PH domain and phosphorylated species because they can be explained if the free phosphates in PBS bind within and occlude the more open PH domain binding pocket in a E416A mutant. In the absence of buffer phosphates, the opened pocket becomes receptive to Ins(3,4,5)P_3 on an enhanced basis. We believe these data suggest that the kindlin-1 PH domain is not evolutionarily adapted to recognize inositol phosphates but some other phosphorylated species. In support of this contention, our structure-based phylogenetic analysis has defined distinct clades related to PH domain function, with the kindlin-1 PH domain clustered away from most canonical inositol phosphate binding proteins among the other kindlins and domains of unknown or non-canonical ligand binding. However our data show that, if PtdInsPs are the native ligand, the isoform-specific salt bridge must first be broken, and perhaps there is an as yet undescribed regulatory mechanism for this. In contrast, the enhanced affinity of kindlin-2 PH domain, which lacks an occluding salt bridge, in PBS may be due to the free phosphates pre-adapting the binding pocket through nonspecific interaction for subsequent Ins(3,4,5)P_3 binding, inducing a subset of the wide-ranging conformational changes known to accompany it (24, 72).

The role of the PH domain C-terminal helix must be considered within the context of the complete kindlin structure, occupying a loop splitting the FERM F2 subdomain into an N-terminal and a C-terminal portion (24). The most highly conserved region of the structure is found in the α1-α2 loop by which the C-terminal α2 helix is routed off the canonical α1 PH helix before it in the sequence (Fig. 2*B*). Localized sequence conservation is also found within the α2 helix itself, in particular at its interface with α1. The α1-α2 loop conservation (especially the sequence Met-Ala-Asp-Ser-Ser-Tyr) is greater even than that within the core of the domain fold (Fig. 3*B*). This suggests that the presentation of the C-terminal helix is critical to its function.

The poor affinity for PtdInsP species found for both kindlin-1 and the other kindlin PH domains is strikingly at variance with published data from kindlin-2 that show binding to PtdIns3,4,5P_3 with low micromolar affinity (24). We are unable to suggest exactly why this is so but note that the dissociation of the kindlin-2 PH domain reported from the biosensor surface was remarkably slow (24). In addition, the authors noted the very slow association of the PH domain to the surface and that aggregation might be a problem for their data (24). The slow association is reflected in the failure of the sensograms reported by Liu *et al.* (24) to reach saturation, and it must be noted that in the case of the kindlin-1 PH domain mutant and kindlin-2 PH domain in HEPES buffer (at least) this was not the case with our data (Fig. 5, *B* and *C*). Considering data presented by Liu *et al.*

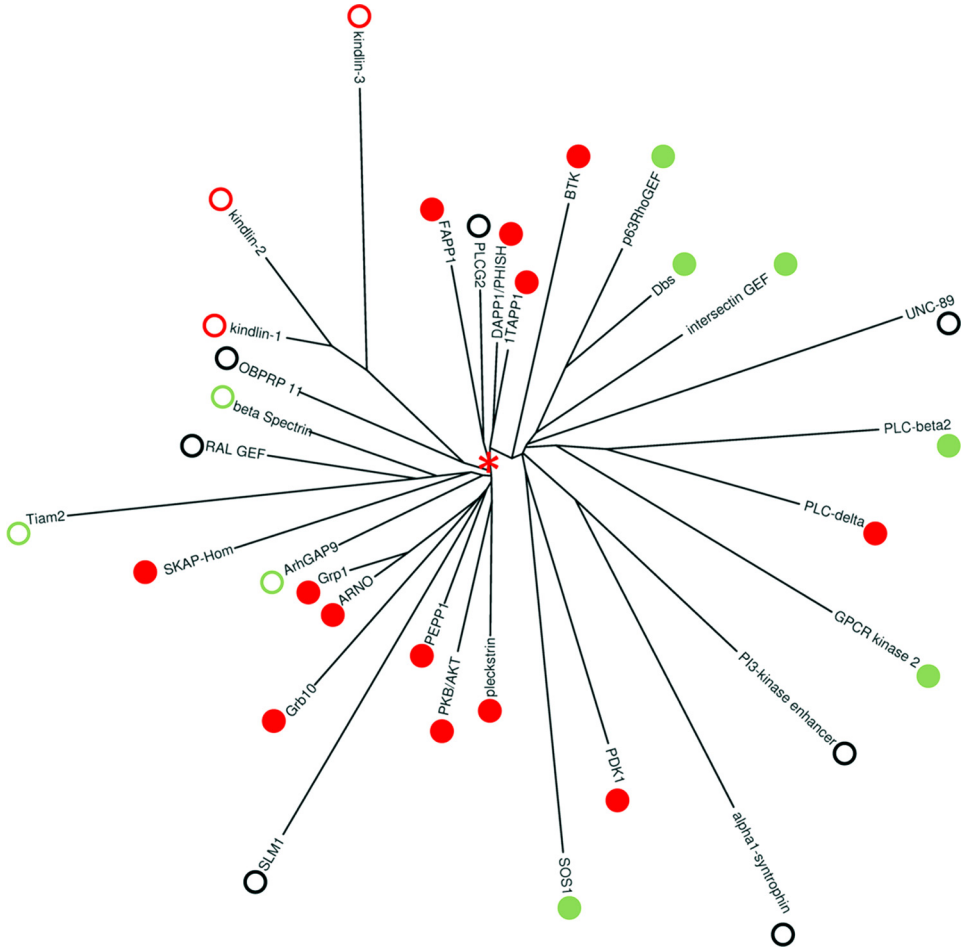

FIGURE 7. **Structure-Based Phylogenetic Analysis of kindlin-1 PH domains and other PH domains.** The structures were superimposed, and a pairwise alignment was carried out using the program SHP (37, 38) to generate an evolutionary distance matrix. *PDK1*, protein-dependent kinase 1 (*H. sapiens*, PDB code 1W1H); pleckstrin (*H. sapiens*, PDB code 2I5F); PKB/AKT, protein kinase B/AKT (*H. sapiens*, PDB code 1UNQ); PEPP1 (*H. sapiens*, 1UPQ); SLM1, phosphatidylinositol 4,5-bisphosphate-binding protein 1 (*Saccharomyces cerevisiae*, PDB code 2NSU); Grb10, growth factor receptor-bound protein 10 (*H. sapiens*, PDB code 2HK0); ARNO, Arf nucleotide binding site opener (*M. musculus*, PDB code 1U27); Grp1, general receptor for phosphoinositides 1 (*M. musculus*, PDB code 1FGY); ArhGAP9, a rho GTPase-activating protein (*H. sapiens*, PDB code 2P0D); SKAP-Hom, Src kinase-associated adaptor protein 1 (*M. musculus*, PDB code 1U5E); Tiam-2, T-lymphoma invasion and metastasis-inducing protein 2 (*M. musculus*, PDB code 3A8P); RalGNF, Ral guanine nucleotide exchange factor (MS0666) (*M. musculus*, PDB code 2DTC): B-spectrin, β spectrin (*M. musculus*, PDB code 1BTN); OBPRP11, oxysterol-binding-related protein 11 (*H. sapiens*, 2D9X); Kind-1, kindlin-1 (*M. musculus*) (this study); Kind-3: kindlin-3 (*H. sapiens*, PDB code 2YS3); Kind-2, kindlin-2 (*H. sapiens*, PDB code 2LK0); FAPP-1, four-phosphate-adaptor protein 1 (*H. sapiens*, PDB code 3RCP); PLCG1, 1-phosphatisylinositol-4,5-bisphosphate phosphodiesterase γ2 (*H. sapiens*, 2W2W); DAPP1/PHISH, dual adaptor of phosphotyrosine and 3-phosphoinositides (*H. sapiens*, PDB code 1FB8); TAPP1, tandem PH domain containing protein 1 (*H. sapiens*, 1EAZ); BTK1, Bruton's tyrosine kinase 1 (*H. sapiens*, PDB code 1B55); PIKE, phosphatidylinositol-3-kinase enhancer protein (*H. sapiens*, PDB code 2RLO); syntrophin, α-1-syntrophin (*M. musculus*, PDB code 2ADZ); p63RhoGEF, p63 Rho guanine nucleotide exchange factor (*M. musculus*, PDB code 2RGN); Dbs, guanine nucleotide exchange factor Dbs (*M. musculus*, PDB code 1KZ7); intersectin, guanine nucleotide exchange factor intersectin (*H. sapiens*, PDB code 1KI1); UNC-89, a muscle protein (*C. elegans*, 1FHO); PLC-β, phospholipase C-β2 (*H. sapiens*, PDB code 2FJU); PLC-δ, phospholipase C-δ (*Rattus norvegicus*, PDB code 1MAI); GPCRK, G protein-coupled receptor kinase 2 (*H. sapiens*, PDB code 1BAK); SOS1, Ras exchanger son of sevenless (*H. sapiens*, PDB code 1AWE). *Red filled circles* indicate canonical PtdInsP binders, *green open circles* indicate non-canonical PtdInsP binders, *open black circles* indicate PH domains of unknown ligand tropism, *green filled circles* indicate protein-binding PH domains, and *red open circles* are used for the kindlin domains. The root of the tree is marked by a *red asterisk*.

(24), it is possible that some nonspecific association to the chip surface occurred and that this enhanced the apparent affinity measured.

The disagreement between our dot-blot data that show a monophosphate PtdInsP tropism for the kindlin-1 PH domain and SPR data that show no interaction between it and PtsIns(3)P or PtdIns(5)P is puzzling. Possible explanations for this difference include the different timescales of the experiments (a 2-h incubation with PH domain was used with the blots) and the random orientation of the lipids in the blot but uniform orientation on the SPR surface. The disagreement perhaps strengthens the impression that PtdInsPs are not native ligands of kindlin-1; in the case of kindlin-2, dot-blot and SPR data were found to be in agreement (24, 25). Note, however, that a difference between our dot-blots and those reported for kindlin-2 PH domain is our use of His_6-tagged proteins, whereas the latter study used ones that were GST-tagged (25). The timescale of the SPR experiments suggests that they may be a more accurate readout on the capacity of kindlin PH domains to interact with PtdInsPs than are lipid overlay assays.

The phylogenetic tree provides context for understanding our data and insight regarding PH family evolutionary conserved features and functions. The PH domains divide phylo-

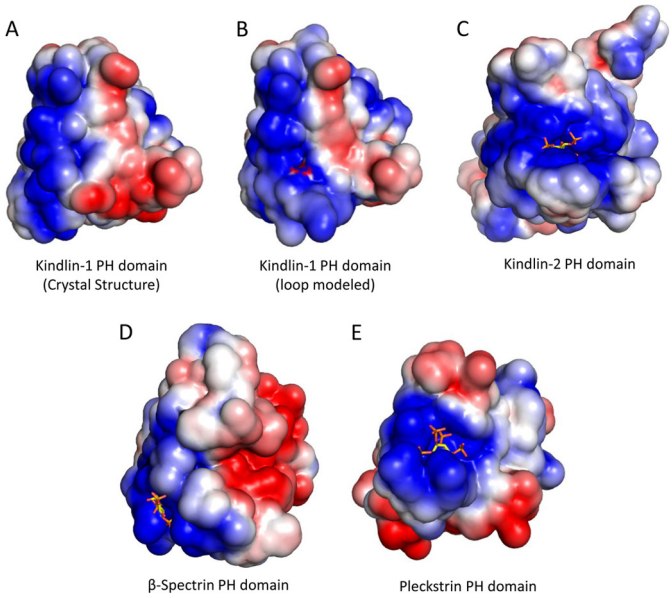

FIGURE 8. **PH domain sruface electrostatic potential.** Representation of the kindlin-1 PH domain crystal structure (*A*), kindlin-1 PH domain complete with modeled disordered loop (see "Experimental Procedures") (*B*), kindlin-2 PH domain (PDB code 2LKO) bound to inositol 1,3,4,5-tetrakisphosphate (24) (*C*), β-spectrin crystal structure (PDB code 1BTN) (*D*), a non-canonical PtdInsP binding module together with D-*myo*-inositol 1,4,5-triphosphate bound rendered in *sticks* and pleckstrin C-terminal PH domain crystal structure (PDB code 2I5F), a canonical PtdInsP binder, together with D-*myo*-inositol 1,2,3,5,6-pentakisphosphate bound rendered in sticks (*E*). The PH domains in all cases are viewed looking down the β-barrel opening and are in identical orientations. Electrostatic calculations were performed using ABPS in PyMol. The electrostatic potential is shaded from −2.5*kT*/*e* (*red*) to +2.5*kT*/*e* (blue).

genetically into two groups, which can be rationalized by one clade showing a preference for phosphorylated inositol ligands and the other for protein ligands (67, 68). A divide thus apparently occurred early on in the development of PH domains that resulted in alternative adaptations. Although protein-protein interaction adaptation can be expected to involve variation over a substantial fraction of the protein surface, variation in the phosphatidylinositol binding capability of the proteins can be the result of very limited substitutions. Thus, the protein-interacting PH domains are widely spaced on their phylogenetic branches, whereas the PtdIns-binding protein branches are tightly clustered. The specific adaptations present in distinct members of the kindlin superfamily perhaps allow them to perform different biological functions in line with their specificity in tissue expression (1, 7). The structure and position of this phylogenetic branch suggests that kindlin PH domains may even be representative of a grouping distinct from both the protein binding and PtdInsP binding domains. However, they are also close to the main canonical PtdInsP binding cluster, and this agrees with reported data for kindlin-2 (24, 25) and the SPR binding assays we report here.

Our work shows that the kindlin-1 PH domain is important for kindlin ability to co-activate integrins. Additionally, our structure provides an atomic description of the kindlin-1 PH domain, and this in conjunction with molecular dynamics and phylogenetic analyses, enabled us to glean insights about the protein function, mechanism of ligand binding, and the physiological relevance of various inositol phosphate substrates.

Acknowledgments—The Oxford Division of Structural Biology is part of the Wellcome Trust Centre for Human Genetics, Wellcome Trust Core Award Grant number 090532/Z/09/Z. We gratefully acknowledge the technical support of David Staunton and Marcus Bridge and the use of the SPR equipment in the Biophysical Facility of the Department of Biochemistry, University of Oxford, and the Sir William Dunn School of Pathology, University of Oxford.

REFERENCES

1. Moser, M., Legate, K. R., Zent, R., and Fässler, R. (2009) The tail of integrins, talin, and kindlins. *Science* **324,** 895–899
2. Anthis, N. J., Wegener, K. L., Critchley, D. R., and Campbell, I. D. (2010) Structural diversity in integrin/talin interactions. *Structure* **18,** 1654–1666
3. Ma, Y. Q., Qin, J., Wu, C., and Plow, E. F. (2008) Kindlin-2 (Mig-2). A co-activator of β3 integrins. *J. Cell Biol.* **181,** 439–446
4. Wegener, K. L., Partridge, A. W., Han, J., Pickford, A. R., Liddington, R. C., Ginsberg, M. H., and Campbell, I. D. (2007) Structural basis of integrin activation by talin. *Cell* **128,** 171–182
5. Harburger, D. S., Bouaouina, M., and Calderwood, D. A. (2009) Kindlin-1 and -2 directly bind the C-terminal region of β integrin cytoplasmic tails and exert integrin-specific activation effects. *J. Biol. Chem.* **284,** 11485–11497
6. Montanez, E., Ussar, S., Schifferer, M., Bösl, M., Zent, R., Moser, M., and Fässler, R. (2008) Kindlin-2 controls bidirectional signaling of integrins. *Genes Dev.* **22,** 1325–1330
7. Ussar, S., Wang, H. V., Linder, S., Fässler, R., and Moser, M. (2006) The Kindlins. Subcellular localization and expression during murine development. *Exp. Cell Res.* **312,** 3142–3151
8. Mackinnon, A. C., Qadota, H., Norman, K. R., Moerman, D. G., and Williams, B. D. (2002) *C. elegans* PAT-4/ILK functions as an adaptor protein within integrin adhesion complexes. *Curr. Biol.* **12,** 787–797
9. Tu, Y., Wu, S., Shi, X., Chen, K., and Wu, C. (2003) Migfilin and Mig-2 link focal adhesions to filamin and the actin cytoskeleton and function in cell shape modulation. *Cell* **113,** 37–47
10. Lai-Cheong, J. E., Ussar, S., Arita, K., Hart, I. R., and McGrath, J. A. (2008) Colocalization of kindlin-1, kindlin-2, and migfilin at keratinocyte focal adhesion and relevance to the pathophysiology of Kindler syndrome. *J. Invest. Dermatol.* **128,** 2156–2165
11. Wu, C. (2005) Migfilin and its binding partners. From cell biology to human diseases. *J. Cell Sci.* **118,** 659–664
12. Kloeker, S., Major, M. B., Calderwood, D. A., Ginsberg, M. H., Jones, D. A., and Beckerle, M. C. (2004) The Kindler syndrome protein is regulated by transforming growth factor-β and involved in integrin-mediated adhesion. *J. Biol. Chem.* **279,** 6824–6833
13. Moser, M., Nieswandt, B., Ussar, S., Pozgajova, M., and Fässler, R. (2008) Kindlin-3 is essential for integrin activation and platelet aggregation. *Nat. Med.* **14,** 325–330
14. Shi, X., Ma, Y. Q., Tu, Y., Chen, K., Wu, S., Fukuda, K., Qin, J., Plow, E. F., and Wu, C. (2007) The MIG-2/integrin interaction strengthens cell-matrix adhesion and modulates cell motility. *J. Biol. Chem.* **282,** 20455–20466
15. Has, C., Herz, C., Zimina, E., Qu, H. Y., He, Y., Zhang, Z. G., Wen, T. T., Gache, Y., Aumailley, M., and Bruckner-Tuderman, L. (2009) Kindlin-1 Is required for RhoGTPase-mediated lamellipodia formation in keratinocytes. *Am. J. Pathol.* **175,** 1442–1452
16. Feng, C., Li, Y. F., Yau, Y. H., Lee, H. S., Tang, X. Y., Xue, Z. H., Zhou, Y. C., Lim, W. M., Cornvik, T. C., Ruedl, C., Shochat, S. G., and Tan, S. M. (2012) Kindlin-3 mediates integrin αLβ2 outside-in signaling, and it interacts with scaffold protein receptor for activated-C kinase 1 (RACK1). *J. Biol. Chem.* **287,** 10714–10726
17. Ussar, S., Moser, M., Widmaier, M., Rognoni, E., Harrer, C., Genzel-Boroviczeny, O., and Fässler, R. (2008) Loss of Kindlin-1 causes skin atrophy and lethal neonatal intestinal epithelial dysfunction. *PLoS Genet.* **4,** e1000289
18. Kern, J. S., Herz, C., Haan, E., Moore, D., Nottelmann, S., von Lilien, T.,

Greiner, P., Schmitt-Graeff, A., Opitz, O. G., Bruckner-Tuderman, L., and Has, C. (2007) Chronic colitis due to an epithelial barrier defect. The role of kindlin-1 isoforms. *J. Pathol.* **213,** 462–470
19. Dowling, J. J., Vreede, A. P., Kim, S., Golden, J., and Feldman, E. L. (2008) Kindlin-2 is required for myocyte elongation and is essential for myogenesis. *BMC Cell Biol.* **9,** 36
20. Moser, M., Bauer, M., Schmid, S., Ruppert, R., Schmidt, S., Sixt, M., Wang, H. V., Sperandio, M., and Fässler, R. (2009) Kindlin-3 is required for β2 integrin-mediated leukocyte adhesion to endothelial cells. *Nat. Med.* **15,** 300–305
21. Svensson, L., Howarth, K., McDowall, A., Patzak, I., Evans, R., Ussar, S., Moser, M., Metin, A., Fried, M., Tomlinson, I., and Hogg, N. (2009) Leukocyte adhesion deficiency-III is caused by mutations in KINDLIN3 affecting integrin activation. *Nat. Med.* **15,** 306–312
22. Malinin, N.L., Zhang, L., Choi, J., Ciocea, A., Razorenova, O., Ma, Y.Q., Podrez, E.A., Tosi, M., Lennon, D.P., Caplan, A.I., Shurin, S.B., Plow, E.F., and Byzova, T.V. (2009) A point mutation in KINDLIN3 ablates activation of three integrin subfamilies in humans. *Nat. Med.* **15,** 313–318
23. Schmidt, S., Nakchbandi, I., Ruppert, R., Kawelke, N., Hess, M. W., Pfaller, K., Jurdic, P., Fässler, R., and Moser, M. (2011) Kindlin-3-mediated signaling from multiple integrin classes is required for osteoclast-mediated bone resorption. *J. Cell Biol.* **192,** 883–897
24. Liu, J., Fukuda, K., Xu, Z., Ma, Y.Q., Hirbawi, J., Mao, X., Wu, C., Plow, E.F., and Qin, J. (2011) Structural basis of phosphoinositide binding to kindlin-2 protein pleckstrin homology domain in regulating integrin activation. *J. Biol. Chem.* **286,** 43334–43342
25. Qu, H., Tu, Y., Shi, X., Larjava, H., Saleem, M. A., Shattil, S. J., Fukuda, K., Qin, J., Kretzler, M., and Wu, C. (2011) Kindlin-2 regulates podocyte adhesion and fibronectin matrix deposition through interactions with phosphoinositides and integrins. *J. Cell Sci.* **124,** 879–891
26. Berrow, N. S., Alderton, D., Sainsbury, S., Nettleship, J., Assenberg, R., Rahman, N., Stuart, D. I., and Owens, R. J. (2007) A versatile ligation-independent cloning method suitable for high-throughput expression screening applications. *Nucleic Acids Res.* **35,** e45
27. Goult, B. T., Bouaouina, M., Harburger, D. S., Bate, N., Patel, B., Anthis, N. J., Campbell, I. D., Calderwood, D. A., Barsukov, I. L., Roberts, G. C., and Critchley, D. R. (2009) The structure of the N terminus of kindlin-1. A domain important for αiibβ3 integrin activation. *J. Mol. Biol.* **394,** 944–956
28. O'Toole, T. E., Katagiri, Y., Faull, R. J., Peter, K., Tamura, R., Quaranta, V., Loftus, J. C., Shattil, S. J., and Ginsberg, M. H. (1994) Integrin cytoplasmic domains mediate inside-out signal transduction. *J. Cell Biol.* **124,** 1047–1059
29. Battye, T. G., Kontogiannis, L., Johnson, O., Powell, H. R., and Leslie, A. G. (2011) iMOSFLM. A new graphical interface for diffraction-image processing with MOSFLM. *Acta Crystallogr. D Biol. Crystallogr.* **67,** 271–281
30. Collaborative Computational Project, Number 4 (1994) The CCP4 suite. Programs for protein crystallography. *Acta Crystallogr. D Biol. Crystallogr.* **50,** 760–763
31. McCoy, A. J., Grosse-Kunstleve, R. W., Adams, P. D., Winn, M. D., Storoni, L. C., and Read, R. J. (2007) Phaser crystallographic software. *J. Appl. Crystallogr.* **40,** 658–674
32. Langer, G., Cohen, S. X., Lamzin, V. S., and Perrakis, A. (2008) Automated macromolecular model building for X-ray crystallography using ARP/wARP version 7. *Nat. Protoc.* **3,** 1171–1179
33. Emsley, P., and Cowtan, K. (2004) Coot. Model-building tools for molecular graphics. *Acta Crystallogr. D Biol. Crystallogr.* **60,** 2126–2132
34. Painter, J., and Merritt, E. A. (2006) Optimal description of a protein structure in terms of multiple groups undergoing TLS motion. *Acta Crystallogr. D Biol. Crystallogr.* **62,** 439–450
35. Chen, V. B., Arendall, W. B., 3rd, Headd, J. J., Keedy, D. A., Immormino, R. M., Kapral, G. J., Murray, L. W., Richardson, J. S., and Richardson, D. C. (2010) MolProbity. All-atom structure validation for macromolecular crystallography. *Acta Crystallogr. D Biol. Crystallogr.* **66,** 12–21
36. Holm, L., and Rosenström, P. (2010) Dali server. Conservation mapping in 3D. *Nucleic acids Res.* **38,** W545–W549
37. Stuart, D. I., Levine, M., Muirhead, H., and Stammers, D. K. (1979) Crystal structure of cat muscle pyruvate kinase at a resolution of 2.6 Å. *J. Mol. Biol.* **134,** 109–142
38. Riffel, N., Harlos, K., Iourin, O., Rao, Z., Kingsman, A., Stuart, D., and Fry, E. (2002) Atomic resolution structure of Moloney murine leukemia virus matrix protein and its relationship to other retroviral matrix proteins. *Structure* **10,** 1627–1636
39. Felsenstein, J. (1997) An alternating least squares approach to inferring phylogenies from pairwise distances. *Syst. Biol.* **46,** 101–111
40. Pettersen, E. F., Goddard, T. D., Huang, C. C., Couch, G. S., Greenblatt, D. M., Meng, E. C., and Ferrin, T. E. (2004) UCSF Chimera. A visualization system for exploratory research and analysis. *J. Comput. Chem.* **25,** 1605–1612
41. Sali, A., and Blundell, T. L. (1993) Comparative protein modelling by satisfaction of spatial restraints. *J. Mol. Biol.* **234,** 779–815
42. Feig, M., Karanicolas, J., and Brooks, C. L., 3rd. (2004) MMTSB Tool Set. Enhanced sampling and multiscale modeling methods for applications in structural biology. *J. Mol. Graph. Model.* **22,** 377–395
43. Hess, B., Kutzner, C., von der Spoel, D., and Lindahl, E. (2008) GROMACS 4. Algorithms for highly efficient, load-balanced, and scalable molecular simulation. *J. Chem. Theory Comput.* **4,** 435–447
44. van Gunsteren, W. F., Billeter, S. R., Eising, A. A., Hunenberger, P. H., Kruger, P., Mark, A. E., Scott, W., and Tironi, I. G. (1996) *Biomolecular Simulation: The GROMOS96 Manual and User Guide*, Biomos & Hochschulverlag AG an der ETH Zurich, Groningen, The Netherlands
45. Kaminski, G. A., Friesner, R. A., Tirado-Rives, J., and Jorgensen, W. L. (2001) Evaluation and reparametrization of the OPLS-AA force field for proteins via comparison with accurate quantum chemical calculations on peptides. *J. Phys. Chem. B* **105,** 6474–6487
46. Hermans, J., Berendsen, H. J. C., Van Gunsteren, W. F., and Postma, J. P. (1984) A consistent empirical potential for water-protein interactions. *Biopolymers* **23,** 1513–1518
47. Jorgensen, W. L., Chandrasekhar, J., Madura, J. D., Impey, R. W., and Klein, M. L. (1983) Comparison of simple potential functions for simulating liquid water. *J. Chem. Phys.* **79,** 926–934
48. Berendsen, H. J. C., Postma, J. P. M., Van Gunsteren, W. F., DiNola, A., and Haak, J. R. (1984) Molecular dynamics with coupling to an external bath. *J. Chem. Phys.* **81,** 3684–3690
49. Parrinello, M., and Rahman, A. (1981) Polymorphic transitions in single crystals. A new molecular dynamics method. *J. Appl. Physiol.* **52,** 7182–7190
50. Nose, K., and Klein, M. L. (1983) Constant pressure molecular dynamics for molecular systems. *Mol. Physiol.* **50,** 1055–1076
51. Hess, B., Becker, H., Berendsen, H. J. C., and Fraaije, J. G. E. M. (1997) LINCS. A linear constraint solver for molecular simulations. *J. Comput. Chem.* **18,** 1463–1472
52. Darden, T., York, D., and Pedersen, L. (1993) Particle mesh Ewald. An N log(N) method for Ewald sums in large systems. *J. Chem. Phys.* **98,** 10089–10092
53. Morris, G. M., Goodsell, D. S., Halliday, R. A., Huey, R., Hart, W. E., Belew, R. K., and Olson, A. J. (1998) Automated docking using a Lamarckian genetic algorithm and empirical binding free energy function. *J. Comput. Chem.* **19,** 1639–1662
54. Huey, R., Morris, G. M., Olson, A. J., and Goodsell, D. S. (2007) A semiempirical free energy force field with charge-based desolvation. *J. Comput. Chem.* **28,** 1145–1152
55. Dumas, J. J., Merithew, E., Sudharshan, E., Rajamani, D., Hayes, S., Lawe, D., Corvera, S., and Lambright, D. G. (2001) Multivalent endosome targeting by homodimeric EEA1. *Mol. Cell* **8,** 947–958
56. Tsujishita, Y., Guo, S., Stolz, L. E., York, J. D., and Hurley, J. H. (2001) Specificity determinants in phosphoinositide dephosphorylation. Crystal structure of an archetypal inositol polyphosphate 5-phosphatase. *Cell* **105,** 379–389
57. Miller, G. J., Wilson, M. P., Majerus, P. W., and Hurley, J. H. (2005) Specificity determinants in inositol polyphosphate synthesis. Crystal structure of inositol 1,3,4-trisphosphate 5/6-kinase. *Mol. Cell* **18,** 201–212
58. Begley, M. J., Taylor, G. S., Brock, M. A., Ghosh, P., Woods, V. L., and Dixon, J. E. (2006) Molecular basis for substrate recognition by MTMR2, a myotubularin family phosphoinositide phosphatase. *Proc. Natl. Acad. Sci. U.S.A.* **103,** 927–932

59. Ferguson, K. M., Lemmon, M. A., Schlessinger, J., and Sigler, P. B. (1995) Structure of the high affinity complex of inositol trisphosphate with a phospholipase C pleckstrin homology domain. *Cell* **83,** 1037–1046
60. Milburn, C. C., Deak, M., Kelly, S. M., Price, N. C., Alessi, D. R., and Van Aalten, D. M. (2003) Binding of phosphatidylinositol 3,4,5-trisphosphate to the pleckstrin homology domain of protein kinase B induces a conformational change. *Biochem. J.* **375,** 531–538
61. Li, C., Xu, L., Wolan, D. W., Wilson, I. A., and Olson, A. J. (2004) Virtual screening of human 5-aminoimidazole-4-carboxamide ribonucleotide transformylase against the NCI diversity set by use of AutoDock to identify novel nonfolate inhibitors. *J. Med. Chem.* **47,** 6681–6690
62. Grosdidier, A., Zoete, V., and Michielin, O. (2011) SwissDock, a protein-small molecule docking web service based on EADock DSS. *Nucleic Acids Res.* **39,** W270–W277
63. Grosdidier, A., Zoete, V., and Michielin, O. (2011) Fast docking using the CHARMM force field with EADock DSS. *J. Comput. Chem.* **32,** 2149–2159
64. Schüttelkopf, A. W., and van Aalten, D. M. (2004) PRODRG. A tool for high-throughput crystallography of protein-ligand complexes. *Acta Crystallogr. D Biol. Crystallogr.* **60,** 1355–1363
65. Thompson, J. D., Higgins, D. G., and Gibson, T. J. (1994) ClustalW. Improving the sensitivity of progressive multiple sequence alignment through sequence weighting, position-specific gap penalties and weight matrix choice. *Nucleic Acids Res.* **22,** 4673–4680
66. Lemmon, M. A., Ferguson, K. M., and Abrams, C. S. (2002) Pleckstrin homology domains and the cytoskeleton. *FEBS Lett.* **513,** 71–76
67. Lemmon, M. A. (2008) Membrane recognition by phospholipid binding domains. *Nat. Rev. Mol. Cell Biol.* **9,** 99–111
68. DiNitto, J. P., and Lambright, D. G. (2006) Membrane and juxtamembrane targeting by PH and PTB domains. *Biochim. Biophys. Acta* **1761,** 850–867
69. Hyvönen, M., Macias, M. J., Nilges, M., Oschkinat, H., Saraste, M., and Wilmanns, M. (1995) Structure of the binding site for inositol phosphates in a PH domain. *EMBO J.* **14,** 4676–4685
70. Thomas, C. C., Deak, M., Alessi, D. R., and van Aalten, D. M. (2002) High-resolution structure of the pleckstrin homology domain of protein kinase B/akt bound to phosphatidylinositol (3,4,5)-trisphosphate. *Curr. Biol.* **12,** 1256–1262
71. Ceccarelli, D. F., Blasutig, I. M., Goudreault, M., Li, Z., Ruston, J., Pawson, T., and Sicheri, F. (2007) Non-canonical interaction of phosphoinositides with pleckstrin homology domains of Tiam1 and ArhGAP9. *J. Biol. Chem.* **282,** 13864–13874
72. Liu, Y., Zhu, Y., Ye, S., and Zhang, R. (2012) Crystal structure of kindlin-2 PH domain reveals a conformational transition for its membrane anchoring and regulation of integrin activation. *Protein Cell* **3,** 434–440
73. Terawaki, S., Kitano, K., Mori, T., Zhai, Y., Higuchi, Y., Itoh, N., Watanabe, T., Kaibuchi, K., and Hakoshima, T. (2010) The PHCCEx domain of Tiam1/2 is a novel protein and membrane binding module. *EMBO J.* **29,** 236–250
74. Cronin, T. C., DiNitto, J. P., Czech, M. P., and Lambright, D. G. (2004) Structural determinants of phosphoinositide selectivity in splice variants of Grp1 family PH domains. *EMBO J.* **23,** 3711–3720
75. Snyder, J. T., Worthylake, D. K., Rossman, K. L., Betts, L., Pruitt, W. M., Siderovski, D. P., Der, C. J., and Sondek, J. (2002) Structural basis for the selective activation of Rho GTPases by Dbl exchange factors. *Nat. Struct. Biol.* **9,** 468–475
76. Worthylake, D. K., Rossman, K. L., and Sondek, J. (2004) Crystal structure of the DH/PH fragment of Dbs without bound GTPase. *Structure* **12,** 1078–1086
77. Worthylake, D. K., Rossman, K. L., and Sondek, J. (2000) Crystal structure of Rac1 in complex with the guanine nucleotide exchange region of Tiam1. *Nature* **408,** 682–688
78. Frech, M., Andjelkovic, M., Ingley, E., Reddy, K. K., Falck, J. R., and Hemmings, B. A. (1997) High affinity binding of inositol phosphates and phosphoinositides to the pleckstrin homology domain of RAC/protein kinase B and their influence on kinase activity. *J. Biol. Chem.* **272,** 8474–8481
79. Dowler, S., Currie, R. A., Campbell, D. G., Deak, M., Kular, G., Downes, C. P., and Alessi, D. R. (2000) Identification of pleckstrin homology domain-containing proteins with novel phosphoinositide binding specificities. *Biochem. J.* **351,** 19–31
80. Baraldi, E., Djinovic Carugo, K., Hyvönen, M., Surdo, P. L., Riley, A. M., Potter, B. V., O'Brien, R., Ladbury, J. E., and Saraste, M. (1999) Structure of the PH domain from Bruton's tyrosine kinase in complex with inositol 1,3,4,5-tetrakisphosphate. *Structure* **7,** 449–460
81. Gouet, P., Courcelle, E., Stuart, D. I., and Métoz, F. (1999) ESPript. Analysis of multiple sequence alignments in PostScript. *Bioinformatics* **15,** 305–308
82. Kumar, S., and Nussinov, R. (2002) Close-range electrostatic interactions in proteins. *Chembiochem* **3,** 604–617